# Water Vapor Variability in Enceladus Plume Spectra from Cassini-VIMS

*A Thesis*

*Presented in Partial Fulfilment of the Requirements for the*

Degree of Master of Science

*with a*

Major in Physics

*in the*

College of Graduate Studies

University of Idaho

*by*

Katie Denny

Major Professor: Matthew Hedman, Ph.D.

Committee Members: Jason Barnes, Ph.D.; Erika Rader, Ph.D.

Department Administrator: John Hiller, Ph.D.

December 2023

# Abstract

The water-vapor content in Enceladus' plume has been difficult to detect and map, being constrained to infrequent observations such as close flybys and occultations. Mapping the plume's water-vapor variations can provide insights into the geological processes that affect the relationship between Enceladus' subsurface ocean and the south polar fissures (tiger stripes). In this thesis, I present the first analysis of detections of water vapor emission in near-infrared Enceladus plume spectra from Cassini's Visual and Infrared Mapping Spectrometer (VIMS). In Chapter 1, I provide a brief background of the Enceladus plume and discuss the motivation for this analysis. Chapter 1 also discusses the format of the VIMS plume data and the methods we used to isolate the water-vapor signal. In Chapter 2, I confirm the existence of the water-vapor emission peak in the near-infrared ($\sim$2.60-2.75$\mu$m) using a data set of 249 spectral cubes with relatively high signal-to-noise ratios. Chapter 2 demonstrates that the signal in the VIMS data is consistent with a real water-vapor feature using model-based predictions and the strength of this water-vapor emission feature corresponds to a line-of-sight column density that is consistent with previous measurements. In Chapter 3, I map water vapor variations by plotting column densities over orbital phase. This chapter also presents an in-depth analysis of variations over orbital phase, variations over years of the Cassini mission, and variations within groups of observations. In Chapter 4, I discuss the implications of this analysis and future missions.

# Acknowledgments

I would first like to thank the members of my committee. Not only was Dr. Matt Hedman an excellent major professor throughout the last two years, but he was also incredibly encouraging and patient as I completed this project. I am grateful for his constant source of inspiration and curiosity towards planetary science, cosmology, and archaeology. I thank Dr. Jason Barnes for his suggestions, collaboration, and expertise towards the iterations of this project. I thank Dr. Erika Rader for giving me the opportunity to attend my first planetary science course and taking time to serve on my committee.

I would like to thank my co-authors, Dr. Dominique Bockelée-Morvan, Dr. Gianrico Filacchione, and Dr. Fabrizio Capaccioni, for their collaboration and suggestions. I would also like to acknowledge Dr. Shannon MacKenzie, Dr. John Spencer, Dr. Sanaz Vahidinia, and Dr. Jay Goguen for showing interest and offering insight into this study.

Next, I would like to thank Himanshi Sharma for her assistance on the beginning coding stages of this project. She was always a comforting and supportive presence in the University of Idaho's physics department.

Acknowledgements to my fellow classmates and friends, Anna Sage Ross-Browning, Cas Tuscon, Jake Hayden, Jonah Haw, and Isiaka Lukman for their unwavering support and much needed board game nights.

Finally, I would like to acknowledge the University of Idaho's physics department and NASA's Cassini Data Analysis Program (Grants: 80NSSC18K1701 and 80NSSC21K0427) for financial support to attend graduate school and study the solar system's most intriguing moon.

# Dedication

To my high school astronomy teacher, Darrick Gray, for showing me how beautiful and exciting studying science can be and helping me be more vocal in the classroom.

To my undergraduate professors, Dr. Daniel McIntosh, Dr. Fred Leibsle, and Dr. Libby Stoddard, for teaching me that communicating science is luminous and interesting. Thank you for believing in me more than I believed in myself.

To my parents, Nancy and Jeff Denny, for always pushing me to never give up on myself and financially backing me through undergrad so I did not have student loans for the rest of my life.

To my best friend and life partner, Cody Halverson, for always supporting me and putting up with my horribly grumpy attitude.

# Table of Contents

# List of Tables

# List of Figures

# Statement of Contribution

The majority of content in this thesis is currently under review for publication in the Planetary Science Journal under the title "Tracing Variations in Enceladus' Water-Vapor Plume Using Near-Infrared Spectra from Cassini-VIMS". For this research, I conducted all of the data analysis, generated all of the figures/tables, and wrote the journal publication. Along with oversight of the data analysis, my advisor, Dr. Matt Hedman, also provided guidance and revisions for the manuscript. Other revisions and suggestions were also provided by three co-authors: Dr. Dominique Bockelée-Morvan, Dr. Gianrico Filacchione, and Dr. Fabrizio Capaccioni. The current citation for this manuscript is shown below:

**Denny, K.E.**, Hedman, M.M., Bockelée-Morvan, D., Filacchione, G., and Capaccioni, F. 2023. Tracing Variations in Enceladus' Water-Vapor Plume Using Near-Infrared Spectra from Cassini-VIMS. *Planetary Science Journal*.

The findings in this thesis contribute to James Webb Space Telescope (JWST) studies involving Enceladus' water plume and torus. Our results confirm the same water vapor emission signal is detected in JWST data and Cassini-VIMS data. The citation for the JWST analysis is shown below:

Villanueva, G. L., Hammel, H. B., Milam, S. N., Kofman, V., Faggi, S., Glein, C. R., Cartwright, R., Roth, L., Hand, K. P., Paganini, L., Spencer, J., Stansberry, J., Holler, B., Rowe-Gurney, N., Protopapa, S., Strazzulla, G., Liuzzi, G., Cruz-Mermy, G., El Moutamid, M., Hedman, M., and **Denny, K.**. JWST Molecular Mapping and Characterization of Enceladus' Water Plume Feeding its Torus. *Nature Astronomy* (2023).

# Chapter 1

# Introduction

Saturn's exceptionally reflective moon, Enceladus, was first discovered in 1789 by William Herschel. Discovered in 1966, Saturn's diffuse E ring composed of ice grains showed a peak brightness intensity near Enceladus providing hints that this moon might supply this material (Dougherty et al., 2018). However, Enceladus' cryovolcano and global subsurface ocean were not confirmed until 2005 when the Cassini spacecraft first observed the moon (see Schenk et al., 2018, and references therein). These discoveries solidified Enceladus' scientific potential, as its large plume allows us to sample the composition of the subsurface ocean through flybys as opposed to a lander. Cassini's sampling of this material yielded estimates of $96 - 99\%$ water and trace amounts of organic compounds (Postberg et al., 2018). Recent studies analyze the likely possibility of phosphorus, a key ingredient for life, existing in Enceladus' ocean (Postberg et al., 2023). These discoveries and the composition estimates show that Enceladus is geologically active and has the potential to harbor life making it an exciting target for future missions.

## 1.1 Enceladus' Particle & Vapor Plume Components

Multiple instruments aboard Cassini observed both the particulate and vapor components of the plume material emerging from four fissures (tiger stripes) located near the south pole of the moon (see Schenk et al., 2018, for recent reviews). Observations of this material have aided in the understanding of the geological processes occurring on Enceladus, however, there are still many questions about how the plume's activity varies over time.

Variations in Enceladus' plume activity on various timescales can provide insights into what is happening beneath the moon's surface. Fluctuations in the plume particle flux have been extensively studied using Cassini's Visual and Infrared Mapping Spectrometer (VIMS) (Hedman et al., 2013) and Imaging Science Subsystem (ISS) data (Nimmo et al., 2014; Ingersoll et al., 2020). These studies show that the overall brightness and particle output of the plume is correlated with Enceladus' position along its eccentric orbit. Specifically, the plume's brightness peaks when Enceladus is furthest from Saturn in its orbit (Hedman et al., 2013; Ingersoll et al., 2020). These trends indicate that the particle flux is correlated with the tidal stresses experienced by Enceladus' South Polar Terrain (Hurford et al., 2009; Nimmo et al., 2014).

The plume's water-vapor variations have been significantly more difficult to document because the water vapor is most clearly observed in relatively short and infrequent observations like occultations and close flybys. These restrictions have led to a debate about whether the vapor plume varies on orbital timescales correlated with particulate component or if it is relatively constant. Occultation data obtained by Cassini's Ultraviolet Imaging Spectrograph (UVIS) indicate that there is a constant vapor flux throughout Enceladus' orbit (Hansen et al., 2020). However, data collected by Cassini's Ion and Neutral Mass Spectrometer (INMS) during close flybys provides evidence of stochastic variations in the plume's gas jets up to a factor of $\sim$10 (Saur et al., 2008; Smith et al., 2010; Teolis et al., 2017).

Enceladus' water-vapor flux can potentially be monitored over a broader range of conditions using near-infrared emission lines. Such lines were recently observed by the James Webb Space Telescope (JWST) (Villanueva et al., 2023), but there is evidence that VIMS can see them as well (Dhingra et al., 2017). The purpose of this project is to use the VIMS observations to quantify the water-vapor concentration of the plume over the course of the Cassini Mission. In doing so, we can answer questions about the plume's gas jets and their interaction with Enceladus' subsurface ocean.

## 1.2 Cassini-VIMS Enceladus Plume Data

VIMS obtained observations of Enceladus and its plume at 352 wavelengths between 0.35 and 5.2 $\mu$m that are packaged as spectral cubes containing two spatial dimensions and one spectral dimension (Brown et al., 2004). We used calibration file RC19 (Clark et al., 2018) and standard routines to convert the raw signal levels to reflectance in units of $I/F$. We computed geometrical parameters like Enceladus' orbital phase (i.e. mean anomaly) based on the timestamp for each observation. It is worth noting that a spectral shift of $\sim$10.4 $nm$ or 0.71 channels occurs over the course of the 13-year Cassini mission (Clark et al., 2018). This spectral shift is almost negligible for this study because the low signal-to-noise ratio and limited spectral resolution of VIMS cubes means that the narrow emission lines are not clearly resolved (see Figure 2.3).

In order to facilitate comparisons among the various plume observations, the data from the infrared channel for each of these cubes were re-projected onto a uniform coordinate system aligned with Enceladus' spin axis and centered on the moon itself (Hedman et al., 2013). An example of the data found in these cubes is shown in Figure 1.1. The *Left* panel shows a map of the plume's brightness in the 2.60-2.75 $\mu$m wavelength band which encompasses the $\nu_1$ and $\nu_3$ vibrational bands of $H_2O$ (Bockelée-Morvan et al., 2015). This map is based on an average of five re-projected VIMS cubes and the bright particle plume is visible extending below Enceladus' south pole. Note that these particular cubes were originally obtained in a mode where each pixel was 0.25 x 0.5 mrad (Hedman et al., 2009), so these pixels appear elongated in the horizontal direction after being re-projected.

While there are a few situations where the water-vapor signal is strong enough to be spatially mapped (Figure 1.1: *Right*, see Section 2.4 for more details), for most of the VIMS observations we can only achieve sufficient signal-to-noise to quantify the water-vapor content of the plume by averaging all the data with the region containing the plume. To ensure consistency, we define the plume area as a region containing 55 pixels

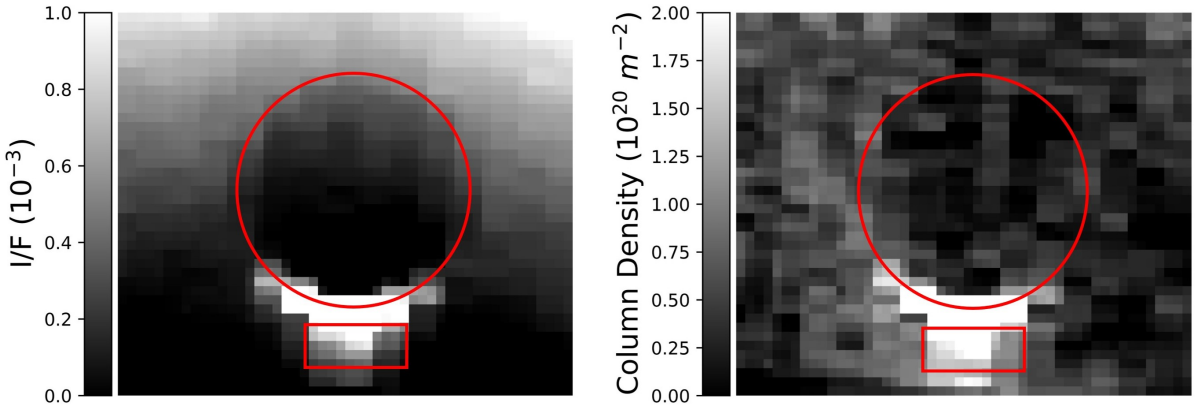


Figure 1.1: *Left:* Map of the plume's brightness at 2.70 $\mu$m derived from an average of five VIMS cubes (V1511798376, V1511800181, V1511800741, V1511801493, and V1511802247). Note that this brightness is mostly due to reflected sunlight from Enceladus' lit limb and the plume particles. The image is oriented so that the plume points downward. *Right:* Map of the water-vapor column density derived from the same averaged image. Column densities were calculated using the average residual values and Equation 2.1. Note that regions of high column density are visible outside the region where the plume particles are bright, which provides evidence that this signal traces a different plume component. The red circles outline Enceladus and the red rectangles show the pixels used for the spectral analysis.

in the re-projected cubes covering altitudes ∼30 km to ∼130 km below Enceladus' South Pole and within ∼120 km of the moon's spin axis (see red rectangles in Figure 1.1). These ranges were selected to avoid contamination from Enceladus' lit limb while still capturing altitudes where the water-vapor signal is expected to be strongest. In particular, the UVIS occultation data indicate that water-vapor column density is strongest at altitudes below 100 km (Hansen et al., 2020). To remove instrumental backgrounds, we subtract the mean signal in a nine pixel region centered at ∼330 km from Enceladus' spin axis and ∼20 km below the south pole. To filter outliers in each cube's average plume spectra, we also calculated standard deviations within each spectral channel and discarded $I/F$ values more than $2\sigma$ away from the median when computing these averages. Finally, we exclude all data in spectral channel 2.564 $\mu$m because it consistently contains outliers throughout the data set even though this channel is not defined as a hot pixel in the VIMS documentation (Clark et al., 2018).

To ensure consistency among our estimates of the plume signal, we only considered cubes that fully covered the selected region and that were obtained at distances within

300,000 km of Enceladus. There were 249 cubes spanning a range of orbital phases and observation times meeting these criteria, which are listed as groups in Table 3.1. A list of the individual 249 spectral cubes can be found in Tables 2.2 - 2.8.

# Chapter 2

# Detection of Water Vapor Emission

The water-vapor signal in the VIMS data is relatively subtle because the instrument's limited spectral sampling ($\approx$ 16.6 nm/band) does not allow individual lines to be clearly detected. Instead the signal appears as a slightly elevated brightness between 2.60 and 2.75 $\mu$m that is superimposed on top of a background spectral slope due to reflected sunlight from the particles in the plume and E ring (Dhingra et al., 2017). We first noticed this slightly elevated brightness in these data in residuals from a Mie model fit to the spectra described in Section 2.1 below. We therefore developed techniques to isolate the potential water-vapor signal from each cube that are described in Section 2.2. In addition, we verified that the relevant spectral feature could indeed be due to water-vapor emission by both comparing the average signal to predictions from the Planetary Spectrum Generator (PSG, see Section 2.3) and checking that the band area of this feature is consistent with the expected average column density of water vapor in the plume (see Section 2.4).

## 2.1 Mie Scattering Models

The first evidence of the water-vapor feature came from examining residuals of Enceladus plume spectra from Mie Scattering models. Mie Scattering models are used for various applications including modeling coma particles from comets (Filacchione et al., 2020). In this study, the Mie models were utilized to model the crystalline water-ice 3.0 $\mu$m absorption feature in the particulate component of the plume. We modeled a data set obtained from Hedman et al. (2009) containing spectra of effective altitudes above the surface of Enceladus processed from a subset of 14 spectral cubes observed in 2005.

In fitting these models, a slight peak appears in the 2.60-2.75 $\mu$m range in some of the spectra, while usually showing up in spectra observed at lower altitudes. The left panel in Figure 2.1 shows the best-fit Mie model for the plume spectra at an altitude of 35 km in the 2.50-3.70 $\mu$m range. The right panel in Figure 2.1 shows the residual brightness produced by subtracting the Mie model from the plume spectra which shows a clear peak. This finding prompted us to expand our analysis to a larger data set of VIMS spectral cubes (see Section 1.2) and develop quadratic fitting models for isolating the water-vapor emission feature from the water-ice absorption spectra (see Section 2.2).

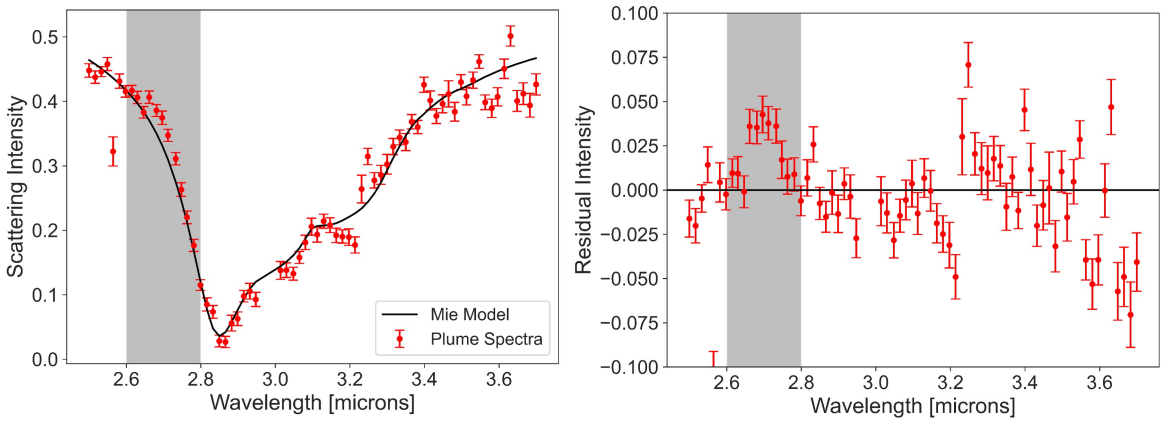


Figure 2.1: Modeling Enceladus plume spectra using Mie Scattering theory. The processed plume spectra were obtained from Hedman et al. (2009). *Left:* shows the best-fit Mie Model for plume spectra observed 35 km above the surface of Enceladus in the 2.5-3.7$\mu$m wavelength range. *Right:* shows the resulting residual intensity after subtracting the Mie model from the spectra. The shaded regions on each plot highlight the wavelength band of interest, a near-infrared region that contains a water vapor emission peak.

## 2.2 Model Fitting & Image Analysis

For this analysis we will focus on the plume signals in the 2.484 $\mu$m - 2.850 $\mu$m wavelength range. These spectra include both the water-vapor signal between 2.60 and 2.75$\mu$m and background trends due to the plume and E-ring particles. These background trends can conveniently be approximated by a low order polynomial, so we can isolate the water-vapor signal by first defining three wavelength bands: 2.484-2.598$\mu$m, 2.615-2.733$\mu$m,

and 2.748-2.850$\mu$m. The middle band contains the eight wavelength channels where we would expect to find the water vapor emission signal. In order to isolate this signal, we fit quadratic polynomials to the data in both surrounding bands (2.484-2.598 $\mu$m and 2.748-2.850 $\mu$m)[1]. These polynomial models are then subtracted from the spectra to produce residuals showing the intensity of water vapor emission in the middle band for each cube.

Figure 2.2 (top panel) shows the non-weighted average spectra of the plume as derived from the entire 249 cube data set (Table 3.1) and the resulting residual $I/F$ brightness (middle panel). Note that a straight average was taken because variations in the strength of the water-vapor feature (see Section 3) are not properly accounted for using weights based on the error bars of individual spectral cubes. The error bars for this spectrum are therefore based on the root mean square residuals about the quadratic trend. The top panel of Figure 2.2 shows a strong slope that is well fit by a quadratic model and can be attributed to the water-ice absorption band in the reflected sunlight from the particles in the plume (Hedman et al., 2009; Dhingra et al., 2017). On top of this trend, a potential water-vapor signal is visible as a slight peak present around 2.60-2.75 $\mu$m. The middle panel shows the residual $I/F$ after subtracting the quadratic fit from the spectra, which isolates the potential water vapor emission feature.

[1] Note that higher order models, such as cubic polynomials, were considered, but these did not significantly change the residuals.

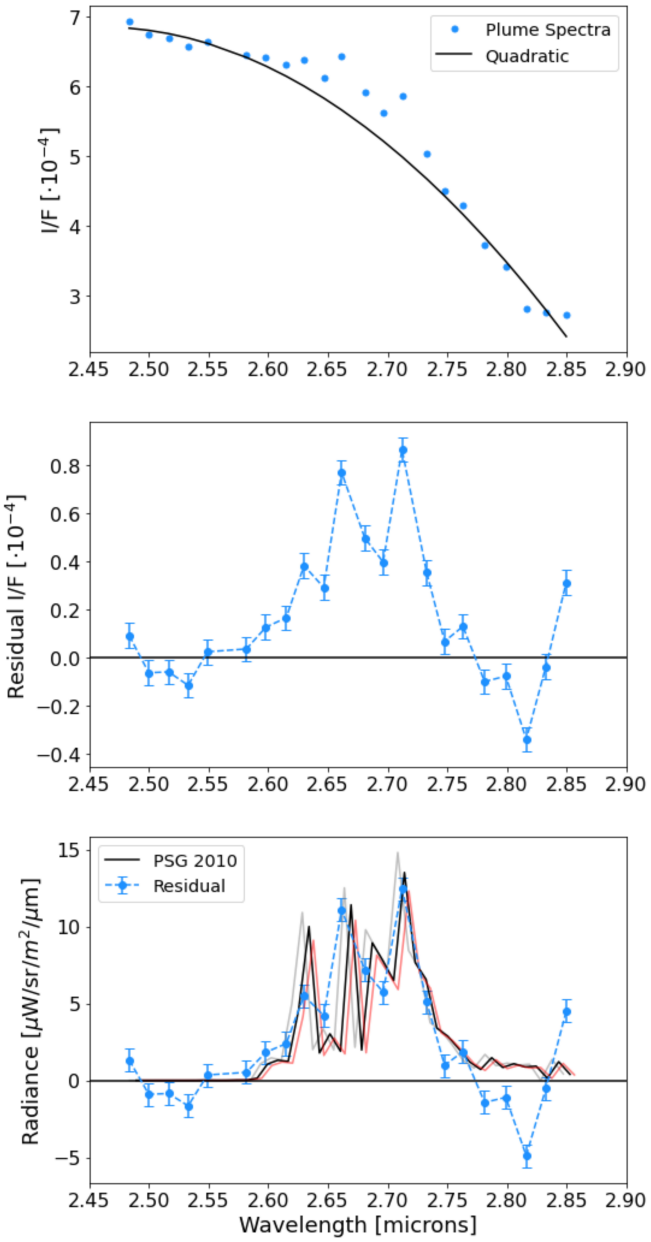


Figure 2.2: The average plume spectra and residual of 249 spectral cubes from Cassini-VIMS observed from 2005 to 2015. The top panel shows the background-subtracted average spectra along with a quadratic fit to the regions between 2.484-2.598 $\mu$m and 2.748-2.850 $\mu$m. The middle panel shows the residual brightness after subtracting the quadratic polynomial. The bottom panel shows the same plume residual compared to the PSG models for 2005 (grey), 2010 (black), and 2015 (red). The wavelength shift in the PSG models was applied using values from Clark et al. (2018) (see Figure 2.3). The models assume a column density of $3.6 \times 10^{19} m^{-2}$, consistent with the best-fit column density based on the feature's band area (see Section 2.4).

## 2.3 Planetary Spectrum Generator

In order to determine if the residual signal shown in Figure 2.2 is compatible with water vapor emission, we compared our observed spectra with predictions from the Planetary Spectrum Generator[2] (PSG). This tool can model spectral features based on various properties related to the celestial body, detector, composition, etc (Villanueva et al., 2018). For this particular study, we assume the Enceladus plume acts similarly to an expanding coma from a comet and consists of only water molecules since estimates of the water vapor abundance are within the 96-99% range (Postberg et al., 2018).

Table 2.1: Planetary Spectrum Generator Parameters

| Parameter | Value |
|---|---|
| Object | S-Enceladus |
| Viewing Geometry | Limb |
| Altitude | 1000 $km$ |
| Atmosphere | Expanding Coma |
| Activity | 3.6 x $10^{19}$ $m^{-2}$ |
| Temperature | 70 K |
| Expansion Velocity | 780 $m/s$ |
| Composition | GSFC[H2O] |
| Abundance | 100% |
| Spectral Range | 2.5-2.9 $\mu$m |
| Resolution (Resolving Power) | 300 |
| Include Molecular Signatures | (Check) |
| Spectrum Intensity Unit | W/sr/$m^2$/$\mu$m |

We use a water-vapor column density of $3.6 \times 10^{19} m^{-2}$, which is consistent with calculations provided in Section 2.4. We also assume a temperature of 70K for the models because this is the equilibrium temperature of ice at Saturn's distance from the sun and it is consistent with the coldest temperatures seen on Enceladus' surface (Spencer et al., 2018). Note that this temperature is different from the rotational temperature of water molecules as quoted in Villanueva et al. (2023). Expansion velocity (also known as jet velocity) was taken from Villanueva et al. (2023). and the Cassini-VIMS resolving power

[2] https://psg.gsfc.nasa.gov

was taken from Brown et al. (2004). The full list of PSG input parameters can be found in Table 2.1. The lower panel in Figure 2.2 shows PSG models from 2005, 2010, and 2015 compared to the average spectrum residual from all 249 spectral cubes (converted to units of Radiance). The PSG model has been applied three times to take into account the reduction of solar flux due to the increase of the heliocentric distance from 2005 to 2015. The spectral shift between the three PSG models shown in the plot corresponds to the wavelength shift in VIMS observations over the Cassini mission (Clark et al., 2018). A more detailed plot of this spectral channel shift can be found in Figure 2.3. Comparing the average residual signal to the three PSG models shows that the shape and intensity of the detected signal are consistent with predicted signal from water-vapor emission lines. This supports the idea that this feature is a real signal from water vapor in the plume.

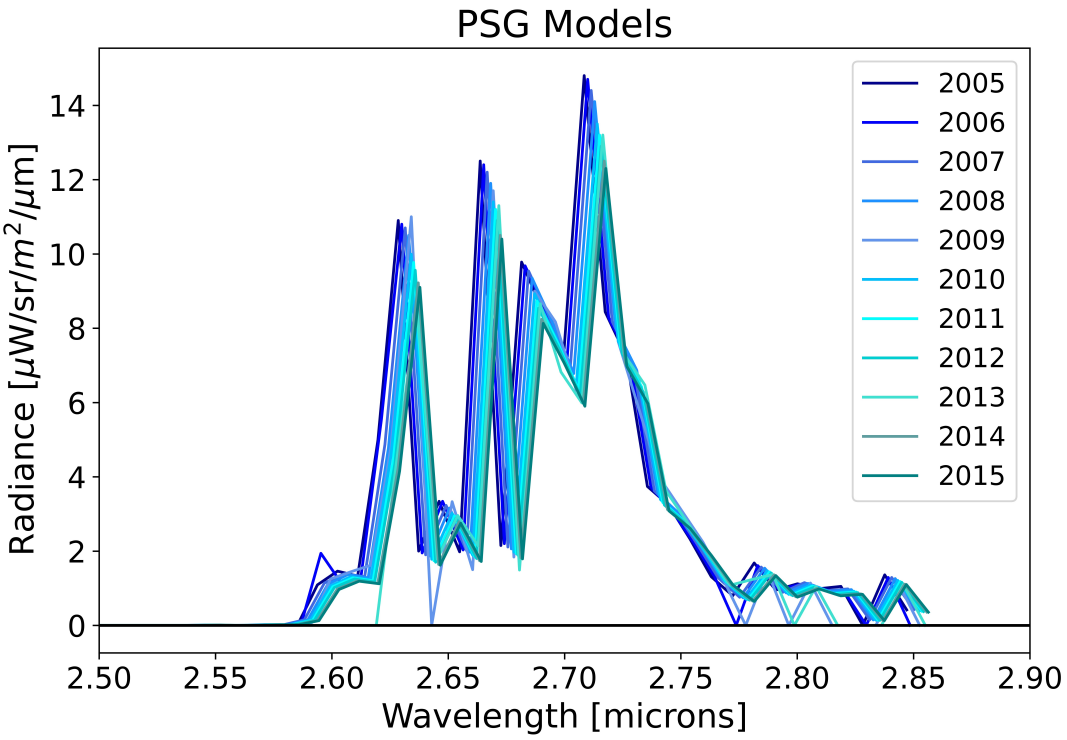


Figure 2.3: Theoretical spectral channel shift of the water vapor emission feature in Cassini-VIMS observations from 2005 to 2015. Spectral shift values were taken from Clark et al. (2018), and the spectral models were produced using the PSG.

## 2.4 Column Density

Another way to validate the water-vapor signal is to estimate the column density of $H_2O$ molecules along the line of sight using the following equation (Bockelée-Morvan et al., 2015).

$$\langle N \rangle = \frac{4\pi I_b}{h\nu g_f} \tag{2.1}$$

where $I_b$ is the band area (signal integrated over the 2.615-2.733 $\mu$m wavelength range), $h$ is Planck's constant, $\nu$ is the central frequency of the band, and $g_f$ is the so-called g-factor or the band emission rate. For this particular band we used the g-factor from Bockelée-Morvan et al. (2015), which gives $g_f = 3.682$ x $10^{-4}$ $s^{-1}$ at 1 AU. To correct for distance, we divided this g-factor by $r^2$ where $r$ is the range between Enceladus and the sun at the time of each observation in Astronomical Units. To convert our residual values to band area, we used the calibration equations from Clark et al. (2018) and solar flux values from the National Renewable Energy Laboratory [3] which are within 6.5% of Thekaekara's solar spectrum (Drummond et al., 1973) used in the VIMS calibration pipeline. Solar flux values were corrected for the sun's range during each observation.

The errors in the column density measurements are calculated using the standard deviation of residual spectral values in the surrounding wavelength bands (2.484-2.598$\mu$m and 2.748-2.850$\mu$m.) and dividing by the square root of the number of spectral channels in the middle band. This should provide a relatively conservative estimate of the uncertainty in the column density that is robust against uncertainties in the models for the background and the signal.

The right panel of Figure 1.1 shows the computed column density for the spectral image produced by averaging five data cubes (V1511800181 - V1511803001). This map shows that the water-vapor signal is more broadly distributed than the particle plume

[3] https://www.nrel.gov/grid/solar-resource/spectra-astm-e490.html

signal, being visible further below Enceladus and being noticeably wider than the particle plume signal visible in the left panel of the same figure. This distinct spatial distribution provides further evidence that this is a real water-vapor signal.

In addition, the average spectrum shown in the bottom panel of Figure 2.2 yields an estimated water vapor column density of $3.6 \pm 0.4 \times 10^{19} m^{-2}$, and for the individual observations the observed signals require column densities of order $10^{20}$ molecules/$m^2$. All column density estimates for individual observations can be found in Tables 2.2 - 2.8 and shown in figures within Chapter 3. These values are consistent with column density measurements made from occultation observations from Cassini's Ultraviolet Imaging Spectrograph (UVIS) which gives values ranging from 9-15 $\times$ $10^{19} m^{-2}$ (Hansen et al., 2020). Villanueva et al. (2023) quotes an average column density of $1.7 \pm 0.1 \times 10^{18} m^{-2}$ from recent JWST observations of Enceladus. The JWST column density is about an order of magnitude lower than ours because the comparatively low spatial resolution of JWST (each pixel being several hundred kilometers wide) means that it can only measure average column densities over broad regions of the plume. By contrast, our data comes within a 100 km of the south polar terrain, where occultation measurements show the plume's column density is much larger (Hansen et al., 2020)[4].

[4] Note that we do not provide estimates of out-gassing rates of the plume material, because these calculations require secure measurements of how the vapor plume's brightness varies with altitude which is hard to extract from our data due to limited signal to noise.

Table 2.2: Column Densities for Spectral Cubes V1511794087-V1635815049

| File | Date | Orbital Phase (°) | $\alpha$ (°) | Range (km) | Solar Range (AU) | $\langle N \rangle$ ($10^{19}$ m$^{-2}$) |
|---|---|---|---|---|---|---|
| V1511794087 | 2005-11-27 | 102.5 | 160.7 | 126873.6 | 9.1 | $8.2 \pm 2.4$ |
| V1511794976 | 2005-11-27 | 104.8 | 161.0 | 128374.5 | 9.1 | $15.0 \pm 4.4$ |
| V1511795992 | 2005-11-27 | 107.9 | 161.1 | 130071.3 | 9.1 | $6.0 \pm 2.5$ |
| V1511796659 | 2005-11-27 | 110.2 | 161.2 | 131177.3 | 9.1 | $-1.5 \pm 2.8$ |
| V1511798376 | 2005-11-27 | 115.4 | 161.3 | 134019.2 | 9.1 | $21.3 \pm 3.2$ |
| V1511800181 | 2005-11-27 | 120.4 | 161.3 | 137068.1 | 9.1 | $12.2 \pm 2.1$ |
| V1511800741 | 2005-11-27 | 122.1 | 161.3 | 138045.0 | 9.1 | $15.0 \pm 1.3$ |
| V1511801493 | 2005-11-27 | 124.6 | 161.3 | 139391.6 | 9.1 | $7.1 \pm 1.9$ |
| V1511802247 | 2005-11-27 | 126.8 | 161.3 | 140794.4 | 9.1 | $15.1 \pm 1.1$ |
| V1511803001 | 2005-11-27 | 129.1 | 161.4 | 142261.8 | 9.1 | $11.3 \pm 2.2$ |
| V1511807379 | 2005-11-27 | 142.0 | 161.4 | 152789.9 | 9.1 | $17.6 \pm 3.9$ |
| V1511807805 | 2005-11-27 | 143.6 | 161.4 | 154063.6 | 9.1 | $9.4 \pm 5.5$ |
| V1511809910 | 2005-11-27 | 149.6 | 161.2 | 161222.1 | 9.1 | $9.5 \pm 5.6$ |
| V1511810387 | 2005-11-27 | 151.0 | 161.2 | 163064.6 | 9.1 | $-15.5 \pm 4.7$ |
| V1556120297 | 2007-04-24 | 77.2 | 155.4 | 184554.5 | 9.2 | $6.2 \pm 4.4$ |
| V1569822293 | 2007-09-30 | 288.8 | 159.0 | 199524.8 | 9.2 | $5.5 \pm 4.4$ |
| V1569822797 | 2007-09-30 | 290.4 | 158.1 | 194771.3 | 9.2 | $8.0 \pm 3.0$ |
| V1569823301 | 2007-09-30 | 291.9 | 157.2 | 190118.4 | 9.2 | $11.1 \pm 1.9$ |
| V1569823933 | 2007-09-30 | 293.4 | 156.0 | 184428.6 | 9.2 | $9.1 \pm 3.4$ |
| V1569824177 | 2007-09-30 | 294.2 | 155.5 | 182275.7 | 9.2 | $-0.9 \pm 2.8$ |
| V1569824421 | 2007-09-30 | 294.9 | 155.0 | 180147.4 | 9.2 | $1.0 \pm 4.3$ |
| V1569824665 | 2007-09-30 | 295.7 | 154.5 | 178044.1 | 9.2 | $1.5 \pm 8.3$ |
| V1569824909 | 2007-09-30 | 296.4 | 153.9 | 175965.8 | 9.2 | $18.8 \pm 2.9$ |
| V1635804522 | 2009-11-01 | 153.0 | 160.3 | 209658.5 | 9.5 | $6.4 \pm 3.3$ |
| V1635804766 | 2009-11-01 | 153.6 | 160.2 | 209343.4 | 9.5 | $43.1 \pm 3.3$ |
| V1635804941 | 2009-11-01 | 154.1 | 160.2 | 209116.9 | 9.5 | $13.1 \pm 7.5$ |
| V1635805116 | 2009-11-01 | 154.6 | 160.1 | 208889.6 | 9.5 | $2.3 \pm 3.4$ |
| V1635805443 | 2009-11-01 | 155.7 | 160.0 | 208462.0 | 9.5 | $-30.9 \pm 8.7$ |
| V1635805657 | 2009-11-01 | 156.3 | 159.9 | 208179.5 | 9.5 | $12.8 \pm 5.8$ |
| V1635806084 | 2009-11-01 | 157.6 | 159.8 | 207607.3 | 9.5 | $-1.5 \pm 6.7$ |
| V1635806434 | 2009-11-01 | 158.6 | 159.7 | 207128.0 | 9.5 | $1.2 \pm 5.7$ |
| V1635806609 | 2009-11-01 | 159.1 | 159.7 | 206884.1 | 9.5 | $-0.2 \pm 5.0$ |
| V1635806784 | 2009-11-01 | 159.7 | 159.7 | 206637.2 | 9.5 | $12.8 \pm 5.0$ |
| V1635806959 | 2009-11-01 | 160.2 | 159.6 | 206386.9 | 9.5 | $-5.7 \pm 6.1$ |
| V1635813829 | 2009-11-01 | 181.0 | 161.4 | 191730.6 | 9.5 | $9.4 \pm 4.0$ |
| V1635814073 | 2009-11-01 | 181.7 | 161.6 | 190968.4 | 9.5 | $1.9 \pm 7.9$ |
| V1635814317 | 2009-11-01 | 182.4 | 161.7 | 190185.7 | 9.5 | $24.1 \pm 8.7$ |
| V1635814561 | 2009-11-01 | 183.2 | 161.9 | 189382.3 | 9.5 | $-7.1 \pm 3.1$ |
| V1635814805 | 2009-11-01 | 183.9 | 162.0 | 188557.7 | 9.5 | $-3.9 \pm 4.4$ |
| V1635815049 | 2009-11-01 | 184.6 | 162.2 | 187711.8 | 9.5 | $-2.1 \pm 3.9$ |

Table 2.3: Column Densities for Spectral Cubes V1635815493-V1671553901

| File | Date | Orbital Phase (°) | $\alpha$ (°) | Range (km) | Solar Range (AU) | $\langle N \rangle$ ($10^{19}$ m$^{-2}$) |
|---|---|---|---|---|---|---|
| V1635815493 | 2009-11-01 | 186.0 | 162.6 | 186116.8 | 9.5 | $-15.4 \pm 8.2$ |
| V1635815737 | 2009-11-01 | 186.7 | 162.7 | 185209.1 | 9.5 | $3.1 \pm 9.2$ |
| V1635815981 | 2009-11-01 | 187.4 | 162.9 | 184279.2 | 9.5 | $12.1 \pm 4.4$ |
| V1635817494 | 2009-11-01 | 192.0 | 164.3 | 178000.8 | 9.5 | $0.6 \pm 8.0$ |
| V1635817738 | 2009-11-01 | 192.7 | 164.5 | 176903.9 | 9.5 | $-37.9 \pm 8.3$ |
| V1652826740 | 2010-05-17 | 367.6 | 157.7 | 290943.6 | 9.5 | $-7.7 \pm 3.3$ |
| V1652826984 | 2010-05-17 | 368.3 | 157.6 | 287429.8 | 9.5 | $7.5 \pm 2.6$ |
| V1652827472 | 2010-05-17 | 369.8 | 157.3 | 280453.2 | 9.5 | $2.0 \pm 1.9$ |
| V1652827842 | 2010-05-17 | 371.0 | 157.0 | 275209.5 | 9.5 | $7.4 \pm 2.9$ |
| V1652828212 | 2010-05-17 | 372.1 | 156.8 | 270006.2 | 9.5 | $8.8 \pm 5.1$ |
| V1652828456 | 2010-05-17 | 372.9 | 156.7 | 266597.1 | 9.5 | $19.6 \pm 4.9$ |
| V1652828700 | 2010-05-17 | 373.6 | 156.5 | 263205.9 | 9.5 | $0.7 \pm 4.8$ |
| V1652829196 | 2010-05-17 | 375.1 | 156.2 | 256368.3 | 9.5 | $-4.8 \pm 3.0$ |
| V1652829440 | 2010-05-17 | 375.9 | 156.1 | 253032.4 | 9.5 | $-2.1 \pm 3.0$ |
| V1652829684 | 2010-05-17 | 376.6 | 155.9 | 249715.1 | 9.5 | $12.9 \pm 3.8$ |
| V1652830180 | 2010-05-17 | 378.1 | 155.7 | 243029.4 | 9.5 | $7.3 \pm 3.3$ |
| V1652830668 | 2010-05-17 | 379.6 | 155.4 | 236528.0 | 9.5 | $9.9 \pm 2.8$ |
| V1660403219 | 2010-08-13 | 336.5 | 161.2 | 293314.5 | 9.5 | $15.1 \pm 5.6$ |
| V1660403463 | 2010-08-13 | 337.3 | 161.0 | 289786.5 | 9.5 | $-6.2 \pm 6.5$ |
| V1660403707 | 2010-08-13 | 338.0 | 160.9 | 286274.9 | 9.5 | $-2.8 \pm 2.8$ |
| V1660406223 | 2010-08-13 | 345.7 | 159.3 | 251068.2 | 9.5 | $-0.6 \pm 7.3$ |
| V1660406711 | 2010-08-13 | 347.2 | 159.0 | 244459.5 | 9.5 | $1.2 \pm 5.8$ |
| V1660406955 | 2010-08-13 | 348.0 | 158.8 | 241183.0 | 9.5 | $15.6 \pm 4.5$ |
| V1660407443 | 2010-08-13 | 349.5 | 158.6 | 234686.1 | 9.5 | $6.4 \pm 3.2$ |
| V1660407687 | 2010-08-13 | 350.2 | 158.4 | 231466.0 | 9.5 | $11.7 \pm 4.5$ |
| V1660407931 | 2010-08-13 | 351.0 | 158.3 | 228265.0 | 9.5 | $10.6 \pm 3.5$ |
| V1663878677 | 2010-09-22 | 452.1 | 159.9 | 255800.6 | 9.6 | $-6.2 \pm 4.3$ |
| V1663879025 | 2010-09-22 | 453.2 | 160.5 | 254471.8 | 9.6 | $9.5 \pm 5.1$ |
| V1663879269 | 2010-09-22 | 453.9 | 160.8 | 253514.8 | 9.6 | $-9.4 \pm 3.6$ |
| V1663879513 | 2010-09-22 | 454.6 | 161.2 | 252536.8 | 9.6 | $23.4 \pm 4.7$ |
| V1663879757 | 2010-09-22 | 455.4 | 161.6 | 251537.9 | 9.6 | $3.3 \pm 4.5$ |
| V1663880001 | 2010-09-22 | 456.1 | 162.0 | 250518.0 | 9.6 | $13.9 \pm 5.8$ |
| V1663880356 | 2010-09-22 | 457.2 | 162.5 | 248996.9 | 9.6 | $2.4 \pm 4.8$ |
| V1663880600 | 2010-09-22 | 458.0 | 162.9 | 247925.7 | 9.6 | $11.2 \pm 6.0$ |
| V1663880844 | 2010-09-22 | 458.7 | 163.3 | 246833.7 | 9.6 | $-34.8 \pm 9.5$ |
| V1663881088 | 2010-09-22 | 459.4 | 163.7 | 245720.9 | 9.6 | $-15.2 \pm 8.9$ |
| V1663881576 | 2010-09-22 | 460.9 | 164.5 | 243433.3 | 9.6 | $-0.9 \pm 7.9$ |
| V1663881820 | 2010-09-22 | 461.7 | 164.9 | 242258.6 | 9.6 | $-32.4 \pm 6.1$ |
| V1671552668 | 2010-12-20 | 358.3 | 163.5 | 156808.5 | 9.6 | $6.3 \pm 5.7$ |
| V1671553901 | 2010-12-20 | 362.1 | 162.1 | 152410.1 | 9.6 | $-16.7 \pm 8.2$ |

Table 2.4: Column Densities for Spectral Cubes V1671557277-V1675108205

| File | Date | Orbital Phase (°) | $\alpha$ (°) | Range (km) | Solar Range (AU) | $\langle N \rangle$ ($10^{19}$ m$^{-2}$) |
|---|---|---|---|---|---|---|
| V1671557277 | 2010-12-20 | 372.3 | 158.7 | 142389.8 | 9.6 | $7.6 \pm 6.7$ |
| V1671558253 | 2010-12-20 | 375.3 | 158.0 | 139839.3 | 9.6 | $13.5 \pm 3.8$ |
| V1671559411 | 2010-12-20 | 379.0 | 157.2 | 136892.9 | 9.6 | $1.2 \pm 7.0$ |
| V1671560658 | 2010-12-20 | 382.8 | 156.5 | 133738.1 | 9.6 | $20.0 \pm 5.6$ |
| V1671561876 | 2010-12-20 | 386.4 | 156.0 | 130589.3 | 9.6 | $-2.2 \pm 3.7$ |
| V1671562852 | 2010-12-20 | 389.4 | 155.8 | 127967.5 | 9.6 | $-3.2 \pm 4.7$ |
| V1671564000 | 2010-12-20 | 392.9 | 155.7 | 124715.0 | 9.6 | $4.3 \pm 3.2$ |
| V1671564976 | 2010-12-20 | 395.9 | 155.7 | 121776.0 | 9.6 | $-5.0 \pm 9.0$ |
| V1671566150 | 2010-12-20 | 399.6 | 155.8 | 117982.9 | 9.6 | $-9.1 \pm 7.2$ |
| V1671567368 | 2010-12-20 | 403.3 | 156.1 | 113717.5 | 9.6 | $-13.3 \pm 4.8$ |
| V1675101079 | 2011-01-30 | 332.7 | 156.7 | 226523.3 | 9.6 | $-4.7 \pm 9.4$ |
| V1675101287 | 2011-01-30 | 333.4 | 156.5 | 225850.2 | 9.6 | $11.6 \pm 7.1$ |
| V1675101532 | 2011-01-30 | 334.1 | 156.2 | 225081.0 | 9.6 | $18.0 \pm 8.5$ |
| V1675101740 | 2011-01-30 | 334.7 | 156.0 | 224450.1 | 9.6 | $25.3 \pm 3.7$ |
| V1675101985 | 2011-01-30 | 335.5 | 155.8 | 223729.6 | 9.6 | $-10.1 \pm 4.9$ |
| V1675102193 | 2011-01-30 | 336.1 | 155.5 | 223139.2 | 9.6 | $20.4 \pm 4.9$ |
| V1675102438 | 2011-01-30 | 336.9 | 155.3 | 222465.2 | 9.6 | $4.7 \pm 2.5$ |
| V1675102646 | 2011-01-30 | 337.5 | 155.1 | 221913.2 | 9.6 | $-14.4 \pm 8.3$ |
| V1675102916 | 2011-01-30 | 338.4 | 154.8 | 221220.6 | 9.6 | $22.8 \pm 3.5$ |
| V1675103124 | 2011-01-30 | 339.0 | 154.6 | 220706.9 | 9.6 | $10.3 \pm 5.7$ |
| V1675103369 | 2011-01-30 | 339.7 | 154.4 | 220121.2 | 9.6 | $-1.9 \pm 8.7$ |
| V1675103822 | 2011-01-30 | 341.1 | 154.0 | 219095.2 | 9.6 | $24.5 \pm 5.1$ |
| V1675104030 | 2011-01-30 | 341.8 | 153.8 | 218647.9 | 9.6 | $3.8 \pm 6.2$ |
| V1675104275 | 2011-01-30 | 342.5 | 153.6 | 218138.0 | 9.6 | $4.2 \pm 7.5$ |
| V1675104483 | 2011-01-30 | 343.2 | 153.4 | 217720.7 | 9.6 | $11.7 \pm 7.2$ |
| V1675104776 | 2011-01-30 | 344.1 | 153.1 | 217153.8 | 9.6 | $13.6 \pm 2.7$ |
| V1675104984 | 2011-01-30 | 344.7 | 153.0 | 216767.1 | 9.6 | $-5.8 \pm 6.3$ |
| V1675105229 | 2011-01-30 | 345.4 | 152.8 | 216326.0 | 9.6 | $9.3 \pm 4.8$ |
| V1675105437 | 2011-01-30 | 346.1 | 152.6 | 215964.6 | 9.6 | $4.4 \pm 3.8$ |
| V1675105682 | 2011-01-30 | 346.8 | 152.4 | 215552.1 | 9.6 | $-26.3 \pm 7.0$ |
| V1675105890 | 2011-01-30 | 347.5 | 152.3 | 215213.9 | 9.6 | $-10.7 \pm 5.5$ |
| V1675106135 | 2011-01-30 | 348.2 | 152.1 | 214827.4 | 9.6 | $-0.4 \pm 7.3$ |
| V1675106343 | 2011-01-30 | 348.9 | 151.9 | 214510.2 | 9.6 | $-13.7 \pm 3.1$ |
| V1675106638 | 2011-01-30 | 349.8 | 151.7 | 214074.5 | 9.6 | $11.3 \pm 4.4$ |
| V1675106846 | 2011-01-30 | 350.4 | 151.6 | 213777.8 | 9.6 | $-23.5 \pm 5.3$ |
| V1675107091 | 2011-01-30 | 351.2 | 151.5 | 213437.7 | 9.6 | $11.6 \pm 4.6$ |
| V1675107544 | 2011-01-30 | 352.5 | 151.2 | 212835.1 | 9.6 | $-3.2 \pm 8.5$ |
| V1675107752 | 2011-01-30 | 353.2 | 151.1 | 212568.8 | 9.6 | $-6.9 \pm 4.4$ |
| V1675107997 | 2011-01-30 | 353.9 | 151.0 | 212261.9 | 9.6 | $-20.5 \pm 5.6$ |
| V1675108205 | 2011-01-30 | 354.6 | 150.9 | 212007.5 | 9.6 | $19.1 \pm 6.0$ |

Table 2.5: Column Densities for Spectral Cubes V1675108515-V1697686836

| File | Date | Orbital Phase (°) | $\alpha$ (°) | Range (km) | Solar Range (AU) | $\langle N \rangle$ ($10^{19}$ m$^{-2}$) |
|---|---|---|---|---|---|---|
| V1675108515 | 2011-01-30 | 355.5 | 150.7 | 211636.5 | 9.6 | $3.4 \pm 8.9$ |
| V1675108723 | 2011-01-30 | 356.2 | 150.6 | 211393.2 | 9.6 | $-9.1 \pm 3.8$ |
| V1675109176 | 2011-01-30 | 357.5 | 150.4 | 210874.7 | 9.6 | $23.2 \pm 7.1$ |
| V1675109629 | 2011-01-30 | 358.9 | 150.3 | 210369.1 | 9.6 | $24.1 \pm 6.2$ |
| V1675110253 | 2011-01-30 | 360.9 | 150.1 | 209685.2 | 9.6 | $6.7 \pm 7.8$ |
| V1675110461 | 2011-01-30 | 361.5 | 150.1 | 209459.2 | 9.6 | $1.6 \pm 6.3$ |
| V1675110914 | 2011-01-30 | 362.9 | 150.0 | 208966.2 | 9.6 | $-2.7 \pm 4.5$ |
| V1675111228 | 2011-01-30 | 363.8 | 149.9 | 208622.4 | 9.6 | $-1.7 \pm 6.1$ |
| V1675111436 | 2011-01-30 | 364.5 | 149.9 | 208393.5 | 9.6 | $-5.5 \pm 5.3$ |
| V1675111681 | 2011-01-30 | 365.2 | 149.9 | 208121.0 | 9.6 | $-1.0 \pm 5.9$ |
| V1675111889 | 2011-01-30 | 365.9 | 149.9 | 207887.8 | 9.6 | $-1.6 \pm 5.2$ |
| V1696147993 | 2011-10-01 | 171.3 | 148.8 | 228707.6 | 9.7 | $1.6 \pm 2.3$ |
| V1696148201 | 2011-10-01 | 172.0 | 148.9 | 225939.0 | 9.7 | $6.0 \pm 4.0$ |
| V1696148409 | 2011-10-01 | 172.6 | 149.0 | 223183.9 | 9.7 | $-4.0 \pm 2.6$ |
| V1696148616 | 2011-10-01 | 173.2 | 149.1 | 220447.3 | 9.7 | $-11.7 \pm 5.4$ |
| V1696148824 | 2011-10-01 | 173.8 | 149.2 | 217719.2 | 9.7 | $9.9 \pm 3.3$ |
| V1696149032 | 2011-10-01 | 174.5 | 149.3 | 215004.9 | 9.7 | $11.7 \pm 3.8$ |
| V1696149239 | 2011-10-01 | 175.1 | 149.4 | 212309.3 | 9.7 | $1.2 \pm 6.5$ |
| V1696149723 | 2011-10-01 | 176.7 | 149.6 | 206077.7 | 9.7 | $-3.3 \pm 2.5$ |
| V1696150058 | 2011-10-01 | 177.7 | 149.8 | 201804.4 | 9.7 | $8.5 \pm 3.4$ |
| V1696150393 | 2011-10-01 | 178.8 | 149.9 | 197567.6 | 9.7 | $-31.5 \pm 6.2$ |
| V1696150728 | 2011-10-01 | 179.8 | 150.1 | 193367.5 | 9.7 | $7.5 \pm 3.4$ |
| V1696151517 | 2011-10-01 | 182.0 | 150.4 | 183619.1 | 9.7 | $-7.4 \pm 3.8$ |
| V1696151725 | 2011-10-01 | 182.6 | 150.4 | 181087.5 | 9.7 | $-2.0 \pm 4.0$ |
| V1696151933 | 2011-10-01 | 183.2 | 150.5 | 178570.2 | 9.7 | $6.4 \pm 4.2$ |
| V1696152140 | 2011-10-01 | 183.8 | 150.6 | 176071.9 | 9.7 | $16.5 \pm 2.9$ |
| V1696152348 | 2011-10-01 | 184.5 | 150.7 | 173583.4 | 9.7 | $0.9 \pm 2.1$ |
| V1696152556 | 2011-10-01 | 185.1 | 150.7 | 171109.5 | 9.7 | $-0.8 \pm 2.8$ |
| V1696152763 | 2011-10-01 | 185.7 | 150.8 | 168654.6 | 9.7 | $-1.7 \pm 2.9$ |
| V1696153294 | 2011-10-01 | 187.5 | 151.0 | 162434.6 | 9.7 | $6.1 \pm 2.9$ |
| V1696153619 | 2011-10-01 | 188.5 | 151.1 | 158674.8 | 9.7 | $21.0 \pm 4.6$ |
| V1696153945 | 2011-10-01 | 189.4 | 151.2 | 154946.4 | 9.7 | $13.4 \pm 3.5$ |
| V1696154270 | 2011-10-01 | 190.4 | 151.3 | 151258.2 | 9.7 | $16.4 \pm 6.3$ |
| V1696154595 | 2011-10-01 | 191.4 | 151.4 | 147605.8 | 9.7 | $19.7 \pm 3.0$ |
| V1696155274 | 2011-10-01 | 193.4 | 151.5 | 140087.2 | 9.7 | $21.1 \pm 2.3$ |
| V1697685856 | 2011-10-19 | 162.4 | 148.2 | 245611.1 | 9.7 | $-3.9 \pm 3.6$ |
| V1697686101 | 2011-10-19 | 163.1 | 148.3 | 242251.8 | 9.7 | $-1.0 \pm 3.3$ |
| V1697686346 | 2011-10-19 | 163.9 | 148.5 | 238910.6 | 9.7 | $5.6 \pm 3.7$ |
| V1697686591 | 2011-10-19 | 164.6 | 148.6 | 235587.5 | 9.7 | $-2.2 \pm 3.2$ |
| V1697686836 | 2011-10-19 | 165.4 | 148.7 | 232282.8 | 9.7 | $15.7 \pm 6.5$ |

Table 2.6: Column Densities for Spectral Cubes V1697687081-V1711543418

| File | Date | Orbital Phase (°) | $\alpha$ (°) | Range (km) | Solar Range (AU) | $\langle N \rangle$ ($10^{19}$ m$^{-2}$) |
|---|---|---|---|---|---|---|
| V1697687081 | 2011-10-19 | 166.1 | 148.8 | 228996.5 | 9.7 | $5.1 \pm 5.3$ |
| V1697687326 | 2011-10-19 | 166.8 | 149.0 | 225728.7 | 9.7 | $-17.1 \pm 1.7$ |
| V1697690755 | 2011-10-19 | 177.2 | 150.6 | 181998.9 | 9.7 | $9.7 \pm 5.9$ |
| V1697691000 | 2011-10-19 | 177.9 | 150.7 | 179021.3 | 9.7 | $17.9 \pm 5.5$ |
| V1697691245 | 2011-10-19 | 178.6 | 150.7 | 176063.6 | 9.7 | $13.8 \pm 6.5$ |
| V1697691757 | 2011-10-19 | 180.2 | 150.9 | 169947.2 | 9.7 | $-1.0 \pm 6.5$ |
| V1697692002 | 2011-10-19 | 180.9 | 151.0 | 167051.5 | 9.7 | $0.2 \pm 6.8$ |
| V1697692247 | 2011-10-19 | 181.6 | 151.1 | 164175.9 | 9.7 | $8.6 \pm 5.8$ |
| V1697692492 | 2011-10-19 | 182.4 | 151.2 | 161320.5 | 9.7 | $20.6 \pm 6.5$ |
| V1697692737 | 2011-10-19 | 183.1 | 151.3 | 158485.2 | 9.7 | $10.4 \pm 5.2$ |
| V1697692982 | 2011-10-19 | 183.8 | 151.4 | 155670.2 | 9.7 | $-11.1 \pm 7.0$ |
| V1697693227 | 2011-10-19 | 184.6 | 151.5 | 152875.3 | 9.7 | $4.3 \pm 7.4$ |
| V1697694471 | 2011-10-19 | 188.3 | 151.8 | 138996.5 | 9.7 | $2.2 \pm 5.7$ |
| V1697694716 | 2011-10-19 | 189.1 | 151.9 | 136324.5 | 9.7 | $15.4 \pm 4.5$ |
| V1699226646 | 2011-11-05 | 161.8 | 148.3 | 223819.7 | 9.7 | $21.2 \pm 6.2$ |
| V1699226984 | 2011-11-05 | 162.8 | 148.4 | 219368.5 | 9.7 | $9.8 \pm 5.4$ |
| V1699227322 | 2011-11-05 | 163.9 | 148.6 | 214953.7 | 9.7 | $-2.4 \pm 5.3$ |
| V1699227660 | 2011-11-05 | 164.9 | 148.7 | 210575.5 | 9.7 | $37.1 \pm 6.9$ |
| V1699227998 | 2011-11-05 | 165.9 | 148.9 | 206234.2 | 9.7 | $-3.0 \pm 4.5$ |
| V1699228542 | 2011-11-05 | 167.5 | 149.1 | 199325.0 | 9.7 | $8.5 \pm 6.2$ |
| V1699228880 | 2011-11-05 | 168.5 | 149.2 | 195081.0 | 9.7 | $-6.7 \pm 8.8$ |
| V1699229218 | 2011-11-05 | 169.6 | 149.4 | 190874.8 | 9.7 | $-12.2 \pm 5.2$ |
| V1699229556 | 2011-11-05 | 170.6 | 149.5 | 186706.4 | 9.7 | $7.0 \pm 4.3$ |
| V1699229894 | 2011-11-05 | 171.6 | 149.6 | 182576.2 | 9.7 | $16.2 \pm 5.1$ |
| V1699230522 | 2011-11-05 | 173.5 | 149.8 | 175004.1 | 9.7 | $2.4 \pm 5.8$ |
| V1699230860 | 2011-11-05 | 174.5 | 150.0 | 170983.6 | 9.7 | $21.1 \pm 8.2$ |
| V1699231198 | 2011-11-05 | 175.5 | 150.1 | 167001.8 | 9.7 | $-13.5 \pm 4.9$ |
| V1699231536 | 2011-11-05 | 176.5 | 150.2 | 163058.8 | 9.7 | $9.7 \pm 8.2$ |
| V1699231874 | 2011-11-05 | 177.5 | 150.3 | 159154.6 | 9.7 | $-0.9 \pm 9.2$ |
| V1711539317 | 2012-03-27 | 115.2 | 155.8 | 295272.6 | 9.7 | $22.6 \pm 3.2$ |
| V1711539605 | 2012-03-27 | 116.1 | 155.9 | 291038.3 | 9.7 | $2.2 \pm 4.4$ |
| V1711539953 | 2012-03-27 | 117.1 | 156.1 | 285936.3 | 9.7 | $-13.7 \pm 6.5$ |
| V1711540241 | 2012-03-27 | 118.0 | 156.2 | 281751.6 | 9.7 | $-13.3 \pm 5.9$ |
| V1711540588 | 2012-03-27 | 119.1 | 156.4 | 276724.9 | 9.7 | $-15.4 \pm 7.3$ |
| V1711540876 | 2012-03-27 | 119.9 | 156.6 | 272591.1 | 9.7 | $-12.1 \pm 5.0$ |
| V1711541224 | 2012-03-27 | 121.0 | 156.7 | 267612.3 | 9.7 | $-0.1 \pm 7.4$ |
| V1711541512 | 2012-03-27 | 121.8 | 156.9 | 263530.7 | 9.7 | $-1.3 \pm 8.3$ |
| V1711542490 | 2012-03-27 | 124.8 | 157.3 | 249821.2 | 9.7 | $-4.5 \pm 5.9$ |
| V1711542778 | 2012-03-27 | 125.7 | 157.5 | 245846.8 | 9.7 | $-13.7 \pm 7.1$ |
| V1711543418 | 2012-03-27 | 127.6 | 157.7 | 237090.1 | 9.7 | $12.6 \pm 3.7$ |

Table 2.7: Column Densities for Spectral Cubes V1711543762-V1713089323

| File | Date | Orbital Phase (°) | $\alpha$ (°) | Range (km) | Solar Range (AU) | $\langle N \rangle$ ($10^{19}$ m$^{-2}$) |
|---|---|---|---|---|---|---|
| V1711543762 | 2012-03-27 | 128.6 | 157.9 | 232428.9 | 9.7 | $-20.0 \pm 4.2$ |
| V1711544399 | 2012-03-27 | 130.6 | 158.1 | 223906.9 | 9.7 | $-1.8 \pm 4.2$ |
| V1711545033 | 2012-03-27 | 132.5 | 158.4 | 215552.1 | 9.7 | $3.9 \pm 4.8$ |
| V1711545321 | 2012-03-27 | 133.4 | 158.5 | 211805.5 | 9.7 | $2.3 \pm 5.6$ |
| V1711545666 | 2012-03-27 | 134.4 | 158.6 | 207339.0 | 9.7 | $-7.8 \pm 6.3$ |
| V1711545954 | 2012-03-27 | 135.3 | 158.7 | 203651.3 | 9.7 | $15.0 \pm 4.1$ |
| V1711546301 | 2012-03-27 | 136.3 | 158.8 | 199230.7 | 9.7 | $25.5 \pm 5.4$ |
| V1711546589 | 2012-03-27 | 137.2 | 158.9 | 195602.7 | 9.7 | $-6.3 \pm 4.6$ |
| V1711546939 | 2012-03-27 | 138.2 | 159.0 | 191217.4 | 9.7 | $29.5 \pm 7.9$ |
| V1711547227 | 2012-03-27 | 139.1 | 159.1 | 187650.2 | 9.7 | $29.5 \pm 5.8$ |
| V1711547571 | 2012-03-27 | 140.1 | 159.2 | 183412.6 | 9.7 | $-8.6 \pm 5.6$ |
| V1711547859 | 2012-03-27 | 141.0 | 159.3 | 179906.1 | 9.7 | $25.8 \pm 8.0$ |
| V1711548206 | 2012-03-27 | 142.1 | 159.4 | 175705.5 | 9.7 | $8.3 \pm 8.0$ |
| V1711548494 | 2012-03-27 | 142.9 | 159.5 | 172260.4 | 9.7 | $-15.5 \pm 6.1$ |
| V1711548846 | 2012-03-27 | 144.0 | 159.6 | 168075.1 | 9.7 | $-3.4 \pm 5.8$ |
| V1711549134 | 2012-03-27 | 144.9 | 159.6 | 164692.3 | 9.7 | $39.8 \pm 8.5$ |
| V1711549477 | 2012-03-27 | 145.9 | 159.7 | 160687.9 | 9.7 | $-11.4 \pm 6.6$ |
| V1711549765 | 2012-03-27 | 146.8 | 159.8 | 157366.7 | 9.7 | $2.6 \pm 6.1$ |
| V1711550111 | 2012-03-27 | 147.8 | 159.9 | 153401.9 | 9.7 | $4.2 \pm 5.8$ |
| V1711550399 | 2012-03-27 | 148.7 | 159.9 | 150142.7 | 9.7 | $-1.5 \pm 6.3$ |
| V1711551038 | 2012-03-27 | 150.6 | 160.1 | 143000.2 | 9.7 | $17.3 \pm 4.2$ |
| V1711551375 | 2012-03-27 | 151.6 | 160.1 | 139284.1 | 9.7 | $-25.1 \pm 10.3$ |
| V1711552021 | 2012-03-27 | 153.6 | 160.2 | 132278.3 | 9.7 | $13.4 \pm 8.1$ |
| V1713081678 | 2012-04-14 | 119.3 | 157.0 | 248755.4 | 9.7 | $-0.5 \pm 8.3$ |
| V1713081923 | 2012-04-14 | 120.0 | 157.1 | 245371.4 | 9.7 | $23.3 \pm 6.8$ |
| V1713082168 | 2012-04-14 | 120.8 | 157.2 | 242005.5 | 9.7 | $12.3 \pm 5.5$ |
| V1713082413 | 2012-04-14 | 121.5 | 157.4 | 238658.0 | 9.7 | $-3.9 \pm 4.5$ |
| V1713082903 | 2012-04-14 | 123.0 | 157.6 | 232018.4 | 9.7 | $-3.4 \pm 7.9$ |
| V1713083212 | 2012-04-14 | 123.9 | 157.7 | 227869.7 | 9.7 | $-4.2 \pm 6.8$ |
| V1713083457 | 2012-04-14 | 124.7 | 157.8 | 224601.5 | 9.7 | $-2.5 \pm 4.2$ |
| V1713083702 | 2012-04-14 | 125.4 | 157.9 | 221352.3 | 9.7 | $21.0 \pm 7.0$ |
| V1713083947 | 2012-04-14 | 126.2 | 158.0 | 218122.2 | 9.7 | $-9.3 \pm 7.3$ |
| V1713084192 | 2012-04-14 | 126.9 | 158.1 | 214911.2 | 9.7 | $3.9 \pm 5.0$ |
| V1713084732 | 2012-04-14 | 128.5 | 158.3 | 207902.2 | 9.7 | $29.9 \pm 8.3$ |
| V1713084977 | 2012-04-14 | 129.3 | 158.3 | 204753.3 | 9.7 | $5.2 \pm 4.9$ |
| V1713085222 | 2012-04-14 | 130.0 | 158.4 | 201624.0 | 9.7 | $10.5 \pm 4.7$ |
| V1713085712 | 2012-04-14 | 131.5 | 158.6 | 195424.6 | 9.7 | $35.8 \pm 10.0$ |
| V1713088408 | 2012-04-14 | 139.6 | 159.4 | 162748.1 | 9.7 | $13.8 \pm 6.2$ |
| V1713088653 | 2012-04-14 | 140.4 | 159.4 | 159900.3 | 9.7 | $-27.7 \pm 3.1$ |
| V1713089323 | 2012-04-14 | 142.4 | 159.6 | 152216.9 | 9.7 | $-14.3 \pm 9.2$ |

Table 2.8: Column Densities for Spectral Cubes V1713089568-V1824760877

| File | Date | Orbital Phase (°) | $\alpha$ (°) | Range (km) | Solar Range (AU) | $\langle N \rangle$ ($10^{19}$ m$^{-2}$) |
|---|---|---|---|---|---|---|
| V1713089568 | 2012-04-14 | 143.1 | 159.6 | 149445.5 | 9.7 | $-11.1 \pm 10.4$ |
| V1713090058 | 2012-04-14 | 144.6 | 159.7 | 143964.0 | 9.7 | $6.2 \pm 7.8$ |
| V1713090554 | 2012-04-14 | 146.1 | 159.8 | 138498.7 | 9.7 | $-16.7 \pm 10.3$ |
| V1713091289 | 2012-04-14 | 148.3 | 159.9 | 130553.2 | 9.7 | $-2.4 \pm 9.9$ |
| V1823537786 | 2015-10-14 | 50.0 | 151.6 | 210144.1 | 10.0 | $7.6 \pm 10.4$ |
| V1823539171 | 2015-10-14 | 54.2 | 150.8 | 218212.5 | 10.0 | $32.6 \pm 5.5$ |
| V1823539863 | 2015-10-14 | 56.4 | 150.3 | 221893.9 | 10.0 | $-29.2 \pm 9.8$ |
| V1823540036 | 2015-10-14 | 56.9 | 150.2 | 222778.1 | 10.0 | $2.0 \pm 7.5$ |
| V1824760877 | 2015-10-28 | 164.4 | 141.8 | 210623.6 | 10.0 | $21.0 \pm 8.0$ |

# Chapter 3

# Water Vapor Variations

Having established that VIMS was able to detect the water vapor content of the plume, we can now use the VIMS observations to search for variations in Enceladus' water vapor activity on a range of different time scales. Residual spectra similar to Figure 2.2 are computed on individual spectral cubes and used to estimate the number of $H_2O$ molecules needed for each cube using the same procedures described in Section 2.4 (see Tables 2.2 - 2.8). As mentioned in Section 2.4, column density errors are calculated using the residuals from the quadratic fits to the background trend. We use these estimates to examine whether the water vapor column densities vary systematically with orbital phase. Next, we present evidence that the column density varies on time scales of less than an hour within groups of observations.

## 3.1 Overview of Observations

Figure 3.1 shows the column density measurements for all 249 spectral cubes in our filtered data set as a function of orbital phase, and the observations are color-coded by the years they were observed. There is no clear pattern in column density fluctuations. To clarify, if the water vapor flux varied with orbital phase like the particle flux, then there would be a clear increase in column density as Enceladus approaches its orbital apocenter, the furthest distance from Saturn along its orbit (180°). Also note that while the data show substantial scatter, the column densities are on average positive, consistent with the detectable signal in the averaged data.

The lower panel of Figure 3.1 shows the variations of the non-weighted average column density estimates of groups of spectral cubes obtained within similar observation

Table 3.1: Average Water Vapor Column Density for Each Observation Group

| File Range | Date | n[a] | Exposure Time[c] (Sec) | Observation Duration[d] (Hours) | $\alpha$ (°) | Range (km) | Orbital Phase[e] (°) | $\langle N \rangle^b$ ($10^{19}$ m$^{-2}$) | $\chi^2_{red}$ |
|---|---|---|---|---|---|---|---|---|---|
| V1511794087-V1511810387 | 2005-11-27 | 14 | 7.9 | 4.6 | 161.2 | 141372.6 | 102.5, 151.0 | $9.3 \pm 1.1$ | 7.6 |
| V1556120297 | 2007-04-24 | 1 | 0.1 | 0.4 | 155.4 | 184554.5 | 77.2 | $6.2 \pm 4.4$ | |
| V1569822293-V1569824909 | 2007-09-30 | 8 | 5.1 | 0.8 | 156.1 | 185659.5 | 288.8, 296.4 | $6.8 \pm 1.2$ | 4.4 |
| V1635804522-V1635817738 | 2009-11-01 | 22 | 14.1 | 3.7 | 161.2 | 197151.8 | 153.0, 192.7 | $1.7 \pm 1.1$ | 10.9 |
| V1652826740-V1652830668 | 2010-05-17 | 12 | 7.7 | 1.1 | 156.6 | 264376.5 | 7.6, 19.6 | $5.1 \pm 1.0$ | 4.8 |
| V1660403219-V1660407931 | 2010-08-13 | 9 | 5.8 | 1.4 | 159.6 | 257005.5 | 336.5, 350.2 | $5.7 \pm 2.6$ | 3.2 |
| V1663878677-V1663881820 | 2010-09-22 | 12 | 7.7 | 0.9 | 162.3 | 249462.4 | 92.2, 101.7 | $-3.0 \pm 2.5$ | 8.4 |
| V1671552668-V1671567368 | 2010-12-20 | 12 | 7.4 | 4.4 | 157.6 | 133235.6 | -1.7, 43.3 | $0.3 \pm 1.7$ | 3.8 |
| V1675101079-V1675111889 | 2011-01-30 | 41 | 26.2 | 3.1 | 152.6 | 215890.0 | -27.3, 5.9 | $3.0 \pm 1.1$ | 7.2 |
| V1696147993-V1696155274 | 2011-10-01 | 24 | 15.4 | 2.1 | 150.2 | 187076.3 | 171.3, 193.4 | $4.4 \pm 0.8$ | 9.3 |
| V1697685856-V1697694716 | 2011-10-19 | 19 | 12.2 | 2.5 | 150.2 | 189015.8 | 162.4, 189.1 | $4.9 \pm 1.5$ | 8.8 |
| V1699226646-V1699231874 | 2011-11-05 | 15 | 9.6 | 1.5 | 149.3 | 190981.2 | 161.8, 177.5 | $6.3 \pm 1.3$ | 5.1 |
| V1711539317-V1711552021 | 2012-03-27 | 34 | 21.8 | 3.6 | 158.4 | 209498.1 | 115.2, 153.6 | $2.3 \pm 0.9$ | 7.4 |
| V1713081678-V1713090058 | 2012-04-14 | 21 | 13.4 | 2.4 | 158.2 | 208633.8 | 119.3, 144.6 | $3.1 \pm 1.4$ | 7.7 |
| V1823539171-V1823540036 | 2015-10-14 | 4 | 2.6 | 0.3 | 150.5 | 220495.3 | 54.2, 56.9 | $3.2 \pm 4.5$ | 11.2 |
| V1824760877 | 2015-10-28 | 1 | 0.6 | 0.1 | 141.8 | 210623.6 | 164.4 | $21.0 \pm 8.0$ | |

[a] The number of spectral cubes in each observation group.
[b] The weighted average group column density is $4.4 \pm 0.3 \times 10^{19}$ m$^{-2}$.
[c] Total exposure time per pixel.
[d] The duration window from the first observation to the last observation.
[e] The minimum and maximum orbital phases for each observation group.

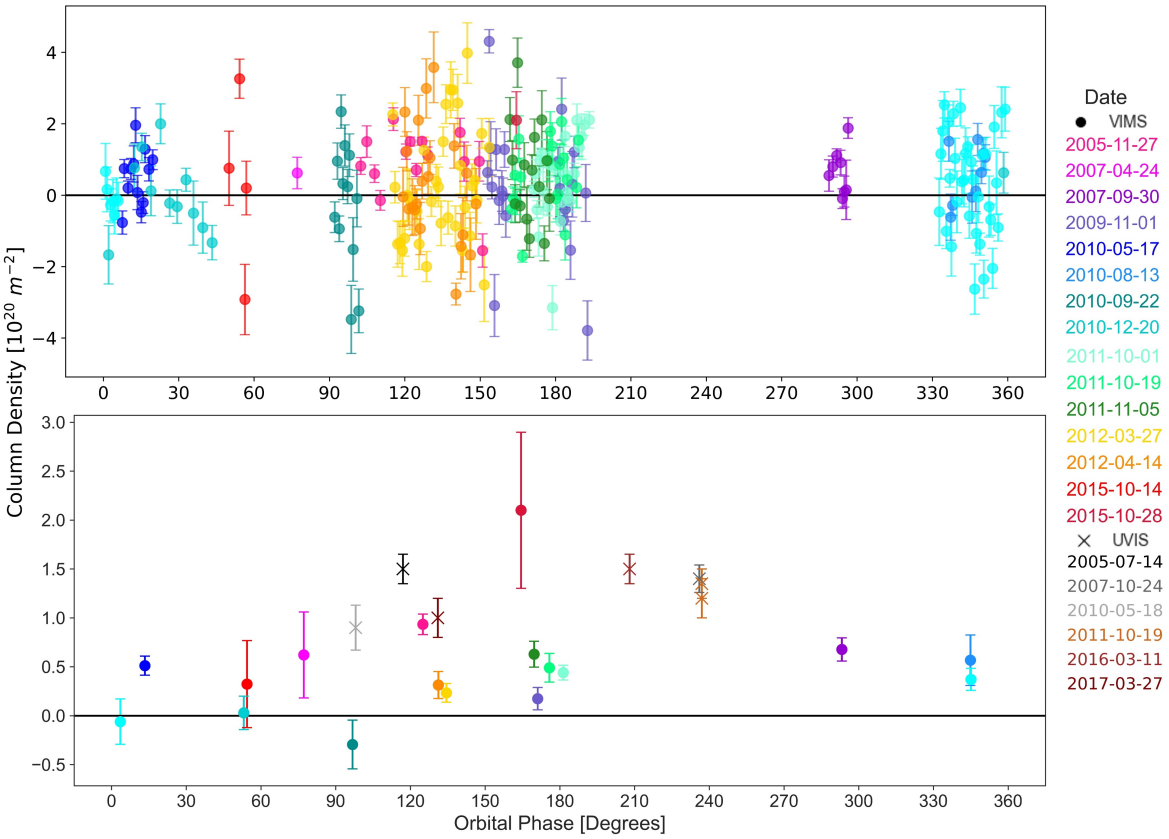


Figure 3.1: Changes in water vapor column density as a function of Enceladus' orbital phase. The top panel shows the column density measurements for 249 spectral cubes (Tables 2.2 - 2.8) with different colors representing the years in which the observations were taken. The bottom panel shows non-weighted average column density estimates for each observation group (Table 3.1). Column density measurements of Enceladus plume occultations observed by UVIS obtained from Hansen et al. (2020) are also shown. There is no evidence for a clear pattern of water vapor column density variations over Enceladus' orbit. Note that although a small fraction of column densities in the top panel are negative, this is likely due to random noise because the signal-to-noise for individual measurements are relatively low. The fact that none of the averaged points in the lower panel are significantly negative is consistent with this idea.

times (see Figures 3.3 and 3.4), along with the estimated water vapor column density measurements derived from UVIS occultation observations (Hansen et al., 2020) (Table 3.1 provides the average column density values for each of these observation groups, along with other properties of the data subsets, note that each group spans no more than five hours of observing time while most of them contain at least eight spectral cubes). The UVIS and VIMS estimates are generally consistent with each other (although the UVIS numbers may be a bit higher on average than the VIMS numbers) and neither shows clear evidence for systematic variations with orbital phase. We therefore agree with Hansen et al. (2020) that the water vapor plume does not show the same systematic activity variations as the particle plume.

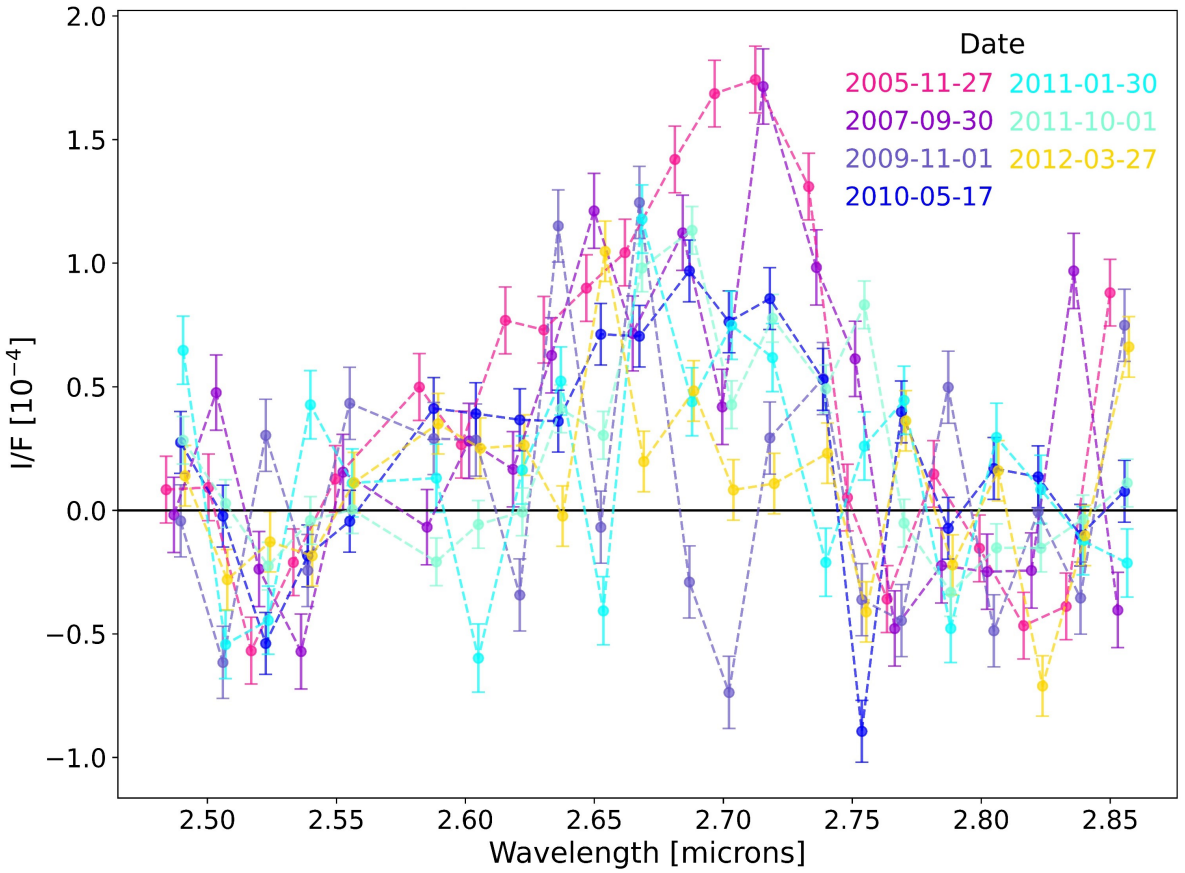


Figure 3.2: The non-weighted average spectral residuals for observation groups with a column density error lower than $1.2\times\ 10^{19}\ m^{-2}$. Each residual is colored by the date the observations were taken corresponding to Figure 3.1.

While Figure 3.1 indicates that there are no obvious trends with orbital phase, it is also important to look at yearly variations and small-scale variations within each observation group. The column density estimates shown in Table 3.1 and the residual plots for individual groups shown in Figures 3.2, 3.3, and 3.4 may reveal hints of yearly variations over the Cassini mission. The water-vapor flux seems to have been particularly high in the VIMS observations taken in 2005 and 2007. Due to relatively low signal to noise, these variations are only marginally significant and could be due to noise if we underestimated our error bars by a factor of two.

## 3.2 Variations Within Groups

In order to investigate short-term variations in the plume, we plot the column density estimates as a function of the orbital phase for each observation group. Figure 3.5 illustrates the water vapor variations for four particularly interesting observation groups in our data set (The remaining observation group plots can be found in Figures 3.6 and 3.7).

The 2005-11-27 group plot shows observations that were previously studied in great detail in Hedman et al. (2009) due to their relatively high signal-to-noise ratios. It is important to note that four out of the five observations between orbital phases of 120° and 130° show the water vapor emission signal clearly in their spectra. While the signal appears to be present in the majority of the cubes, the scatter among the observations is larger than their formal error bars, and the average signal derived from the middle five cubes is significantly higher than that from the average of the earlier and later cubes.

The 2007-09-30 group shows evidence for a possible dip in the water-vapor flux between 294° and 296°, which spans a time of order 10 minutes. This indicates that there may be very fast variations in the vapor plume that can be detected within groups with relatively high signal-to-noise ratios.

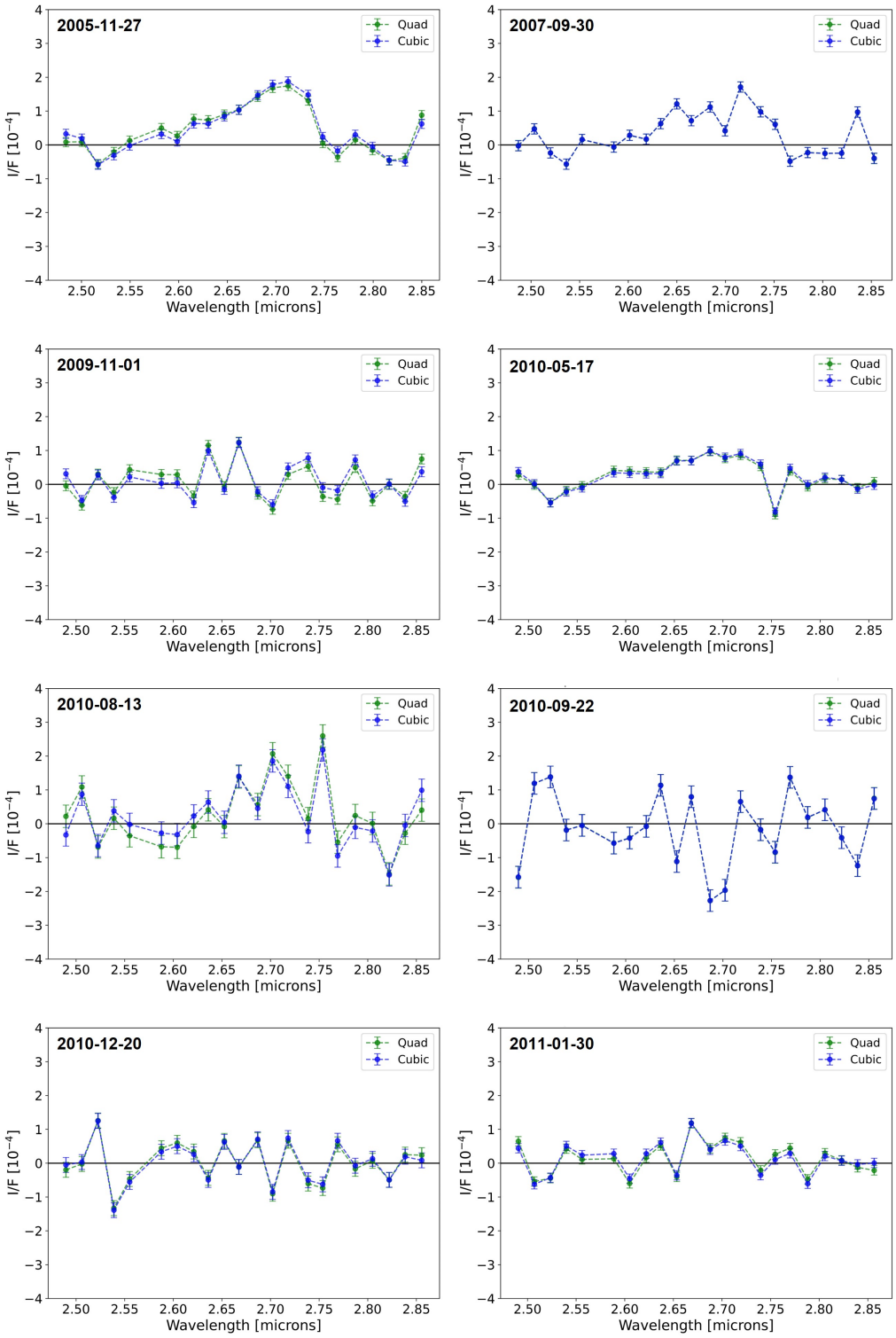


Figure 3.3: Residual Spectra for groups 2005-11-27 through 2011-01-30.

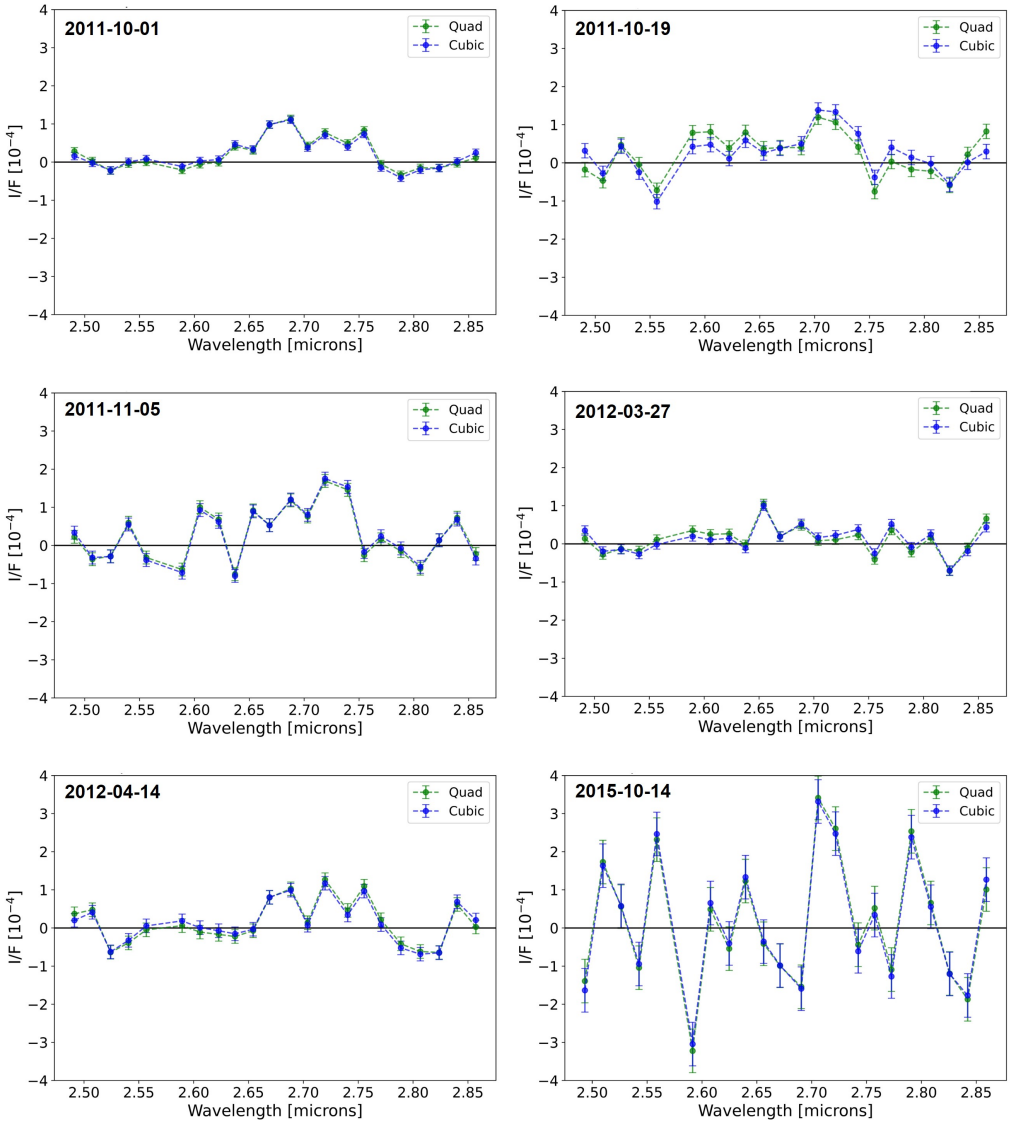


Figure 3.4: Residual Spectra for groups 2011-10-01 through 2015-10-14.

The 2011-10-01 group shows a possible increase in the vapor plume activity between 185° and 195° in a duration of 30 minutes. If this increase is real, the rise in water-vapor flux after Enceladus passes apocenter is interesting because the particle flux would be decreasing in this orbital phase range (Ingersoll et al., 2020; Sharma et al., 2023).

Finally, the 2012-03-27 group maps an interesting result that occurs between orbital phases 135° and 143°. The vapor output tends to bifurcate in this region between relatively large column density measurements and negative ones. Analysis of the individual

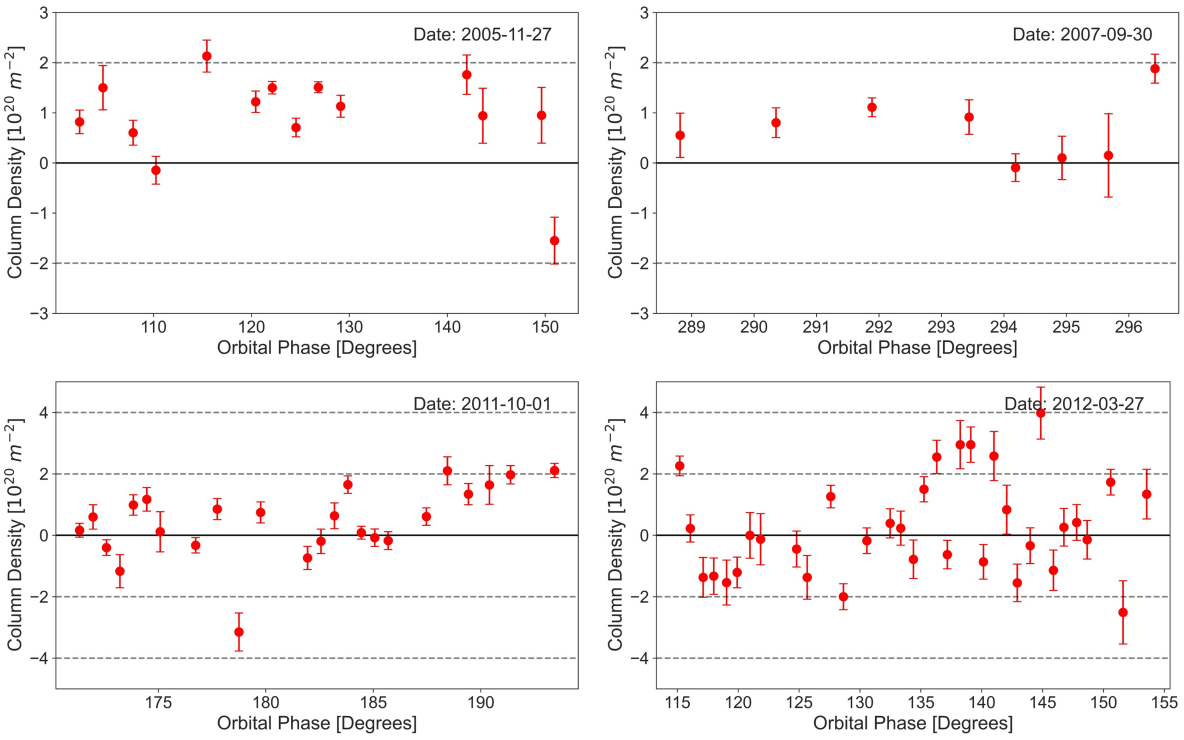


Figure 3.5: Column density variations plotted over the orbital phase in four different observation groups. *2005-11-27:* Variations in the subset of observations analyzed in Hedman et al. (2009). With good signal-to-noise ratios, this group consistently shows the water vapor signal in the middle five observations. *2007-09-30 & 2011-10-01:* Two examples of column density strengths increasing or decreasing within one hour. *2012-03-27:* Represents an interesting result of column density variation between orbital phases 135° and 145°. This region shows that two different sets of observations show different trends in the same orbital range with one being positive and one negative.

spectra of the observations in this orbital phase range shows no clear cause for this odd pattern. While the signal-to-noise ratios in this observation group are fairly low, some spectra exhibit clear emission peaks while others do not.

Figures 3.6 and 3.7 show the column density variations of the remaining groups excluding the two with only one spectral cube. Other details of these groups can be found in Table 3.1 and information on individual cubes can be found in Tables 2.2 - 2.8. These data suggest that the plume's vapor activity potentially varies on short timescales. Note that most of our groups do not have high enough signal-to-noise to adequately map small-scale variations (see Figure 3.5: 2012-03-27). However, given we used relatively conservative error bars in this analysis, the variations in the groups with good signal-to-noise ratios are large enough to merit further investigation with future observations.

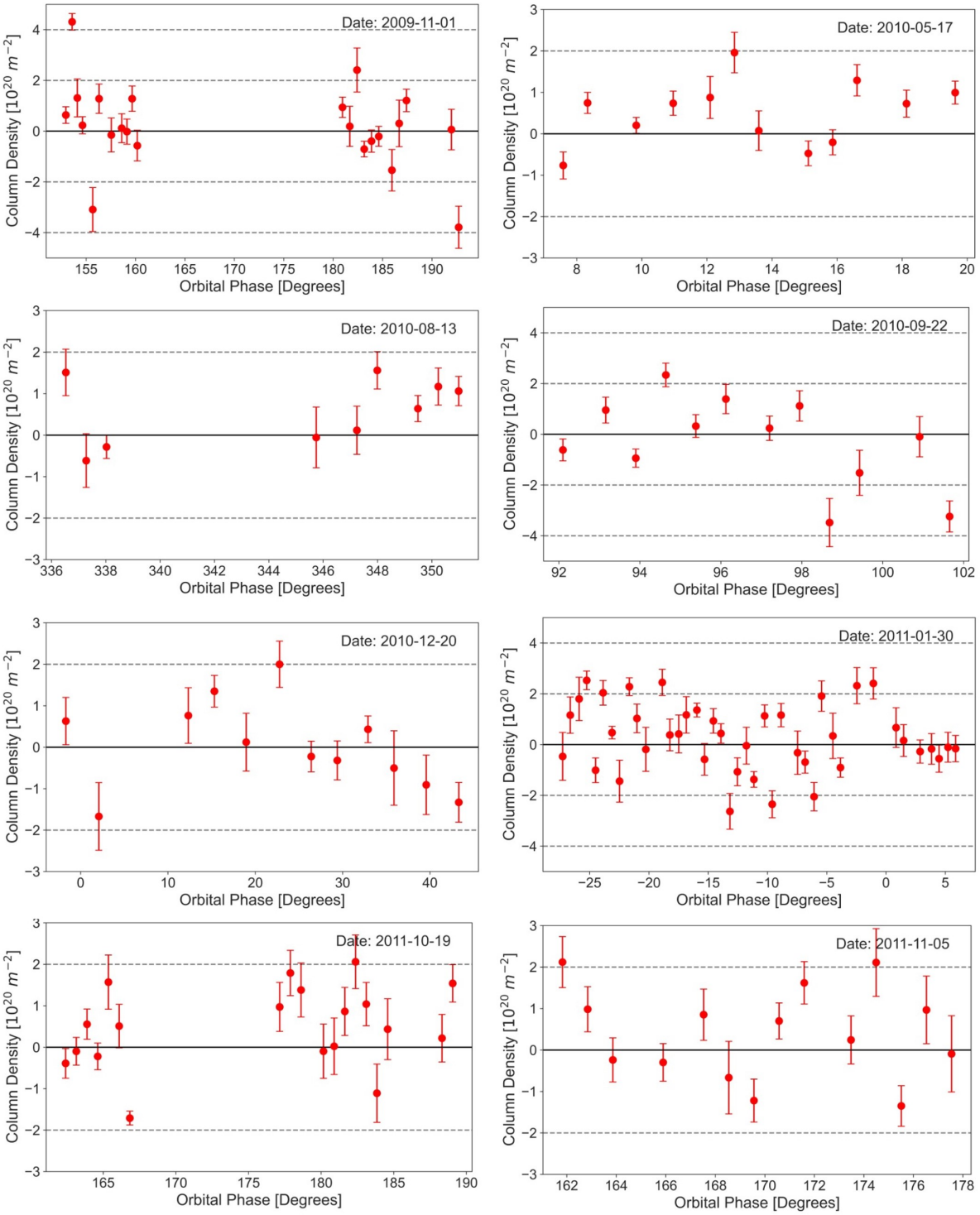


Figure 3.6: Column density variations for groups 2009-11-01 through 2011-11-05. Variations in groups 2005-11-27, 2007-09-30, and 2011-10-01 can be found in Figure 3.5.

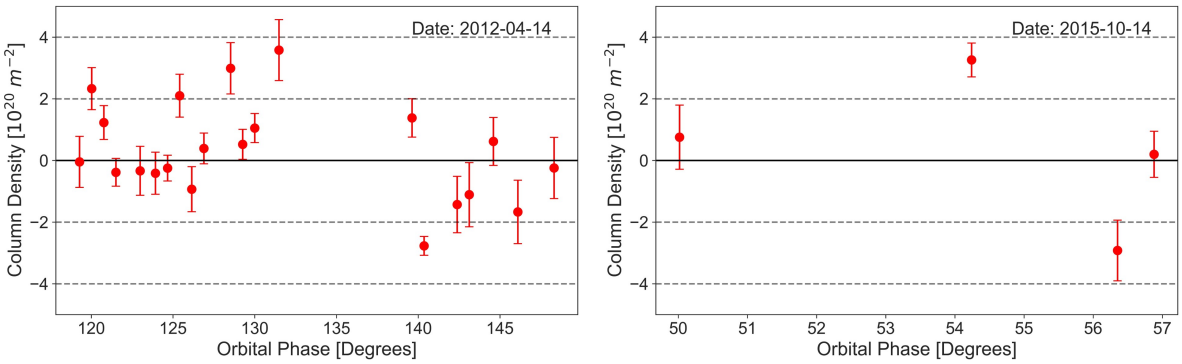


Figure 3.7: Column density variations for groups 2012-04-14 and 2015-10-14. Variations in group 2012-03-27 can be found in Figure 3.5.

## 3.3 Statistical Analysis

To evaluate the reliability of these water vapor variations plotted in Figure 3.1, we conducted a $\chi^2$ analysis of the column density values in the observation groups. Table 3.1 lists the reduced $\chi^2$ for each group of data points and because each value is significantly larger than one, variations within each group tend to be greater than the error variance. For all groups consisting of multiple spectral cubes, the probabilities to exceed associated with the $\chi^2$ values is equal to or much less than 0.01%.

Comparing these individual group values to the total data set $\chi^2$ of $\sim$4, we see that the total data set of column densities shows variance similar to or smaller than the variance of the individual groups. This result implies that there are significant variations among the groups, but these fluctuations are smaller than the variations within most of the observation groups, and are likely just residual short-term variations. To estimate another $\chi^2$ statistic over all the groups, we multiply error values by the square root of each group's $\chi^2$ value with a resulting total value of $\sim$0.6. This value demonstrates that the statistically significant excess variance among observation groups can be attributed to the observed short-term variations within each group.

# Chapter 4

# Discussion & Conclusions

This thesis analyzes Cassini-VIMS near-infrared observations of Enceladus' plume for water vapor emission detections and attempts to bridge gaps in our knowledge of the vapor plume's variability. In the following paragraphs, I summarize and discuss the conclusions from Chapters 2 and 3 which contain the evidence of the water vapor emission detections and the water vapor variations, respectively. To conclude, I will discuss the implications of these results on future missions and studies.

Chapter 2 provides strong evidence that the 2.7 $\mu$m water-vapor emission feature is detectable in Cassini-VIMS near-infrared observations, and these data are consistent with previous UVIS measurements of the plume's vapor column density. Cassini-VIMS was not originally thought to thoroughly detect and resolve water vapor emission even though hints of emission line detections were previously theorized (Dhingra et al., 2017). First detections of water vapor emission were identified using Mie models which shows that the signal appears as a superimposed brightness on top of a background spectral slope (Section 2.1). Using standard polynomial models, we successfully isolated the emission feature in the 2.60-2.75 $\mu$m wavelength range (Section 2.2). Sections 2.3 and 2.4 use two different tools/techniques to confirm the strength of this signal. Comparing residual spectra to PSG water vapor emission models verifies that the signal we detect is consistent with water vapor emission lines. Column density estimates of the strength of this signal are consistent with UVIS studies further confirming that we are detecting water vapor. These results give us access to a data set of 249 Cassini-VIMS observations in which we can use to map water vapor variations.

Our previous knowledge of water vapor fluctuations in Enceladus' plume have been constrained to relatively short and infrequent observations which has led to a debate

about whether the vapor plume's variability is constant (Hansen et al., 2020) or if there are significant fluctuations that are possibly driven by tidal forces (Saur et al., 2008; Smith et al., 2010; Teolis et al., 2017). Chapter 3 utilizes a more extensive data set and analysis to help bridge the gap between these contradicting theories. Section 3.1 confirms that the plume's vapor content does not vary dramatically with orbital phase, which agrees with Hansen et al. (2020). Hints of variation over yearly timescales exist (Figures 3.3 and 3.4). We also find evidence that hints of the plume's vapor content may vary on time scales of around an hour (Section 3.2), but we are only confident of these variations in the groups with the highest signal-to-noise. These results suggests that there is a difference between the tidal variation of the plume's particle flux and the fluctuations in the plume's vapor content. Therefore, the variation in the water-vapor plume is complicated by other geological processes occurring within the fissures. Our detections of minimal variation over orbital phase and small-scale variations in observation groups could be consistent with individual plume jets turning on and off as suggested by Hansen et al. (2020) and studied by Portyankina et al. (2022). This analysis could potentially provide constraints on the frequency and durations of these jet events.

With the launch of JWST, we now have the capabilities to detect water vapor emission in Enceladus' plume with greater spectral resolution. This has already been demonstrated in Villanueva et al. (2023) showing that not only can we detect Enceladus' vapor plume but we can spatially map the torus it forms around Saturn. This confirms that future JWST observations could contribute a deeper understanding of the fluctuations of water-vapor content. However, these future observations would need to be longer or more frequent to adequately map water vapor variations. Not only will these future studies answer questions about the geological processes that govern Enceladus and its cryovolcano, but these could also address broader inquiries about other subsurface ocean worlds like Europa.

# References

Bockelée-Morvan, D., Debout, V., Erard, S., et al. 2015, , 583, A6, doi: 10.1051/0004-6361/201526303

Brown, R. H., Baines, K. H., Bellucci, G., et al. 2004, , 115, 111, doi: 10.1007/s11214-004-1453-x

Clark, R. N., Brown, R. H., Lytle, D. M., & Hedman, M. 2018, NASA Planetary Data System

Dhingra, D., Hedman, M. M., Clark, R. N., & Nicholson, P. D. 2017, , 292, 1, doi: 10.1016/j.icarus.2017.03.002

Dougherty, M. K., Buratti, B. J., Seidelmann, P. K., & Spencer, J. R. 2018, in Enceladus and the Icy Moons of Saturn, ed. P. M. Schenk, R. N. Clark, C. J. A. Howett, A. J. Verbiscer, & J. H. Waite, 3, doi: 10.2458/azu_uapress_9780816537075-ch001

Drummond, A., Drummond, A., Thekaekara, M., & of Environmental Sciences, I. 1973, The Extraterrestrial Solar Spectrum (Institute of Environmental Sciences). https://books.google.com/books?id=Z4TvAAAAMAAJ

Filacchione, G., Capaccioni, F., Ciarniello, M., et al. 2020, , 578, 49, doi: 10.1038/s41586-020-1960-2

Hansen, C. J., Esposito, L. W., Colwell, J. E., et al. 2020, , 344, 113461, doi: 10.1016/j.icarus.2019.113461

Hedman, M. M., Nicholson, P. D., Showalter, M. R., et al. 2009, , 693, 1749, doi: 10.1088/0004-637X/693/2/1749

Hedman, M. M., Gosmeyer, C. M., Nicholson, P. D., et al. 2013, , 500, 182, doi: 10.1038/nature12371

Hurford, T. A., Bills, B. G., Helfenstein, P., et al. 2009, , 203, 541, doi: 10.1016/j.icarus.2009.04.025

Ingersoll, A. P., Ewald, S. P., & Trumbo, S. K. 2020, , 344, 113345, doi: 10.1016/j.icarus.2019.06.006

Nimmo, F., Porco, C., & Mitchell, C. 2014, , 148, 46, doi: 10.1088/0004-6256/148/3/46

Portyankina, G., Esposito, L. W., Aye, K.-M., Hansen, C. J., & Ali, A. 2022, , 383, 114918, doi: 10.1016/j.icarus.2022.114918

Postberg, F., Clark, R. N., Hansen, C. J., et al. 2018, in Enceladus and the Icy Moons of Saturn, ed. P. M. Schenk, R. N. Clark, C. J. A. Howett, A. J. Verbiscer, & J. H. Waite, 129, doi: 10.2458/azu_uapress_9780816537075-ch007

Postberg, F., Sekine, Y., Klenner, F., et al. 2023, , 618, 489, doi: 10.1038/s41586-023-05987-9

Saur, J., Schilling, N., Neubauer, F. M., et al. 2008, , 35, L20105, doi: 10.1029/2008GL035811

Schenk, P., White, O. L., Byrne, P. K., & Moore, J. M. 2018, in Enceladus and the Icy Moons of Saturn, ed. P. M. Schenk, R. N. Clark, C. J. A. Howett, A. J. Verbiscer, & J. H. Waite, 237, doi: 10.2458/azu_uapress_9780816537075-ch012

Sharma, H., Hedman, M. M., & Vahidinia, S. 2023, arXiv e-prints, arXiv:2305.13489, doi: 10.48550/arXiv.2305.13489

Smith, H. T., Johnson, R. E., Perry, M. E., et al. 2010, Journal of Geophysical Research (Space Physics), 115, A10252, doi: 10.1029/2009JA015184

Spencer, J. R., Nimmo, F., Ingersoll, A. P., et al. 2018, in Enceladus and the Icy Moons of Saturn, ed. P. M. Schenk, R. N. Clark, C. J. A. Howett, A. J. Verbiscer, & J. H. Waite, 163, doi: 10.2458/azu_uapress_9780816537075-ch008

Teolis, B. D., Perry, M. E., Hansen, C. J., et al. 2017, Astrobiology, 17, 926, doi: 10.1089/ast.2017.1647

Villanueva, G. L., Smith, M. D., Protopapa, S., Faggi, S., & Mandell, A. M. 2018, , 217, 86, doi: 10.1016/j.jqsrt.2018.05.023

Villanueva, G. L., Hammel, H. B., Milam, S. N., et al. 2023, arXiv e-prints, arXiv:2305.18678, doi: 10.48550/arXiv.2305.18678